AY 101, The Physics of Stars, Fall 2015
Lecture 1 of week 1

- Judy Cohen (jlc@astro.caltech.edu)
- TA: Denise Schmitz (ds@astro.caltech.edu)

- Class hours: Monday 4-5, wed. 9-10, Friday 2-3 pm

Basics I

- Lectures will be white board +
  some PowerPoint for graphics and images.
- Will try to highlight most important concepts/aspects/ equations and relationships.
- Class web page: TBD – will post notes, homeworks, solutions etc
- **Speak Up!** -> questions & interaction.
  Never feel a question may be too stupid to ask!
  Let's make this class a dialogue!

Policies & Rules

- Grade: 70% homework/lab work, 30% final exam.
- Homework should take about 6 hours to complete.
- Homework sets handed out on Friday, due next monday
- Late homework: Extensions with health center note or granted under special circumstances by TAs/lecturer – otherwise 10% of your score per day late.
- Oral midterm (20 minute conversation, pass/fail).
- Final will be take-home, closed book, one 8.5 x 11" sheet with equations/notes on both sides allowed.
- Homework: Honor Code applies!
  - **Science is a team sport**: work in groups, but hand in your very own write up that you fully understand.
  - Do not look at solutions from previous years and/or solutions available on the web.

Literature

- Primary (-> get this book! Must read!):
  LeBlanc,
  An Introduction to Stellar Astrophysics
- Secondary:
  - Hansen, Kawaler, Trimble, *Stellar Interiors.*
  - Philipps, *Physics of Stars.*
  - Kippenhahn & Weigert, *Stellar Structure and Evolution.*
  - Böhm-Vitense, *Stellar Astrophysics Vol. 2 and 3.*
  - Gray, *The Observation and Analysis of Stellar Photospheres.*
  - Rutten, *Radiative Transfer in Stellar Atmospheres.*

Rough Syllabus

- Intro, underlying physics, basic properties of stars
- Star formation
- Radiative transfer, stellar atmospheres
- Stellar interiors
- Stellar evolution, nucleosynthesis, end stages
- Binary evolution
- Supernova explosions

1. Historical Notes for Ay 123

1.1. Nuclear Physics

First nuclear reaction observed by Rutherford in 1919. α-particles emitted by radioactive decay of naturally radioactive Po reacting with nitrogen gas. Po, discovered to be radioactive by the Curies in 1898, has no stable isotopes. ^{209}Po has a half life of 102 years, the longest of any of the Po isotopes It decays into $^{4}He +^{205} Pb$. The α particle is detected through ^{14}N + ^{4}He $\rightarrow^{17}$O + proton.

Understanding of nuclear fission reactions - Hahn and Strassman 1939

First nuclear reactions using accelerated particles, not naturally energetic particles (from radioactive decays), 1932, Cockcroft and Walton

p−p chain worked out by Hans Bethe in 1939 (Nobel prize, 1969)

triple α process (3He $\rightarrow^{12}$C) Salpeter and Hoyle (1952 through 1954)

Prediction of behavior of nuclear reaction rates – Willy Fowler, Nobel prize 1983

Measurement of many nuclear reaction rates – Kellogg Radiation Lab at Caltech, through early 1990s.

1.2. Stellar Spectroscopy and Modelling

Saha – theory of ionization of atoms – 1921

Payne (Cecelia Payne Gaposchkin) applied this to stars and analyzed spectra for stellar abundances, first one to realize that stars are mostly H, Harvard, 1925. First woman tenured faculty member at Harvard.

Unsold - early model stellar atmospheres, 1938

Wildt – (1937) poor agreement of early model stellar atmospheres with real life, suggested missing H^- opacity, which in fact dominates opacity in stars like the Sun

1.3. Progress in Computation and Instrumentation

Progress in this field was highly dependent on improvements in computational capability and a steady trend of bigger telescopes with better instrumentation probing a wider range of wavelengths.

Fig. 1.— "Computers" working at Harvard College Observatory in 1890.

2. Early Famous Women Astronomers

Annie Jump Cannon – worked with Pickering at Harvard College Observatory, did most of the classifications for the Henry Draper Catalog, her job title was "computer".

Henrietta Leavitt – worked as an assistant to Baade at the Mount Wilson Observatory. In 1912 she discovered the period – luminosity law for Cepheids from measuring plates of the Magellanic Clouds

Cecelia Payne Gaposchkin – see above, she worked out the theory of stellar spectra based on the Saha equation, including the dependence of Balmer and other lines on spectral type.

Beatrice Tinsley – (1970s) worked on spectra and evolution of galaxies. She was a research associate at University of Texas, Austin, then a professor at Yale.

3. What is a star ?

Self gravitating sphere (or almost sphere) of gas with a finite definable radius, not easily deformed, not like a cloud in the Earth's atmosphere

Nuclear reactions occur at least to the point where ^{3}He is produced.

radiates energy into the surrounding medium. Jupiter also does this, some internal heat is generated due to radioactive decays, but that is much less than the energy it receives from the Sun. Jupiter is not a star.

4. Stars as Physics Laboratories

Here we demonstrate that conditions are routinely achieved in stars which cannot be achieved in physics laboratories on the Earth, and hence by studying the properties of stars we probe regimes of physical parameters that cannot be reached any other way. The opposite extreme is often reached in the interstellar medium, same idea.

Temperature T(ISM) $\sim 3 - 10$K, T(Sun, center) $\sim 20 \times 10^6$ K, T(Sun, surface) ~ 6000 K, T(Earth, surface) ~ 300K

T(lab) from 0.1 K (for very small volumes only, < 10 cm^3) up to 100,000 K, but the latter, only instantaneously, as in an explosion

Pressure Earth's atmosphere at sea level = 760 mm of Hg = 1×10^6 dyne cm^{-2} (1 mm of Hg = 1 torr, a good vacuum on Earth $\sim 10^{-7}$ torr $\sim 10^{-4}$ dyne cm^{-2}

Sun - P(surface) $\sim 10^4$ dyne cm^{-2}, P(center) $\sim 10^{17}$ dyne cm^{-2}, P(ISM) $\sim 10^{-14}$ dyne cm^{-2}

Number Density (N = mean number density, units atoms (or molecules, or other particles)/cm^3).

N(ISM) ~ 1 atom/cm^3, N(Earth atmosphere, near sea level) $\sim 3 \times 10^{19}$ molecules/cm^3, N(Sun, outer atmosphere) $\sim 5 \times 10^{16}$ atoms/cm^3, N(neutron star, center) $\sim 10^{26}$ neutrons/cm^3.

Density (ρ) Air(Earth's atmosphere, sea level) $\sim 10^{-3}$ gm/cm^3. Water 1 gm/cm^3, lead 2.2 gm/cm^3, ISM 2×10^{-24} gm/cm^3, Sun(center) 100 gm/cm^3, Neutron star (mean density) $\gtrsim 2 \times 10^{12}$ gm/cm^3.

Timescales Age of Earth (radioactive dating) $\sim 3 \times 10^9$ yr, Life on Earth (fossils) $\sim 6 \times 10^8$ yr, Supernova explosion < 1 minute, Nuclear reaction timescale, radiation interaction < 1

sec to 10^9 yr, Lab time scale < 1 sec to 20 yr.

New physics ! nuclear reactions, energy production, degeneracy, equations of state at high P and ρ, neutrino physics...

Some numbers relevant to planets

M(Earth) $\sim 3 \times 10^{-6}$ M(Sun), M(Jupiter) $\sim 1/1000$ M(sun), total mass of 9 planets ~ 450 M(Earth) $\sim 1/1000$ M(Sun)

Total angular momentum of planets $\sim 3 \times 10^{50}$ gm cm^2/sec, Solar angular momentum (almost all from its rotation) $\sim 1.6 \times 10^{48}$ gm cm^2/sec, 1/200 that of the 9 planets.

The Vogt-Russell Conjecture

The properties of a star depend only on M, X, Y, Z, t, which are mass, fractional abundance of H, of He, of elements heavier than He (so $X + Y + Z = 1$), and time (i.e. age).

These variables determine the observed parameters L, R, T_{eff}, g, which are luminosity, radius, effective temperature and surface gravity.

Other potential parameters which have a minor effect (at least in most circumstances) include Ω, B, which are angular velocity (rotation) and magnetic field strength.

Stellar Distances

Direct measurement via parallax - angle subtended by the orbit of the Earth around the Sun. The mean distance to the Sun (the mean radius of the Earth's orbit) is called the astronomical unit (AU). 1 AU = 1.5×10^{13} cm. At a distance of 1 parcsec (1 pc) 1 AU subtends 1 arcsec, so, using the small angle approximation, 1 pc = 1 AU/1 arcsec (in radians) = $1.5 \times 10^{13} \times (57.2 \times 3600) = 3.08 \times 10^{18}$ cm.

Movie illustrating parallax:
www.astronomy.ohio-state.edu/ pogge/Ast162/Movies/parallax.html (from Richard Pogge)

We now introduce the concept of proper motion, as stellar positions change through both parallax and proper motion, and astrometric programs seek to measure both of these.. Since stars move around with random motions within our Galaxy as well as rotate around its center, there are two components to a star's motion relative to the Sun. The first is the velocity along the line of sight, the radial velocity, v_r, which can be measured through the Doppler effect. The second is the motion perpendicular to the line of sight, i.e. in the plane of the sky. This motion, called "proper motion", can be detected as the position of the star on the sky will change with time, moving linearly with time in a fixed direction. Thus the parallax is a small annual oscillation over the larger and constant with time proper motion.

The proper motion(μ) as seen on the sky in units of radians/sec is $\mu = v_T/d = vsin(\phi)/d = v_r tan(\phi)$, where v_T is the tangential projection of the velocity, d is the distance to the object, and ϕ is the angle between the velocity vector and the line of sight. Putting in the appropriate constants, we find that $\mu = v_t/4.74d$, where v_t is given in km/sec, d in pc, and μ in arcsec/yr.

The angular resolution of a telescope on the surface of the Earth is limited to about 1 arcsec by turbulence and thermal variations in the Earth's atmosphere. Only with specialized

techniques can this limit be overcome.

Best centroiding of image of a bright point source: aboue 1/100 of the image size. So from the Earth's surface, we can measure a parallax of 0.01 arcsec or larger, corresponding to distances of 100 pc or smaller. At larger distances, we must rely on indirect estimates based on calibrated properties, such as the period luminosity relationship of Cepheid variables, the peak brightness of supernovae, etc.

Telescopes in space are not affected by this, and the size of the image of distant point source that they produce is limited by diffraction; their performance is not degraded by the Earth's atmosphere. In such a case, $\theta_d \sim 1.2\lambda/D(tel)$, where λ is the wavelength of observation, $D(tel)$ is the diameter of the telescope primary mirror, and θ_d is the diffraction image size (in radians). If can again centroid to 1/100 of the image size, than for $D(tel) \sim 4$ m, distances out to 10^4 pc (10 kpc) can be determined.

Astrometric space missions: Hipparcos (ESA satellite) - small telescope, 29 cm diameter primary mirror, 1 mas accuracy positions for 118,000 stars (mostly $V < 7.9$ mag) launched 1989, took data for about 4 years, years of data analysis produced the Hipparcos catalog, released in 1997. Many arguements about how accurate the parallaxes in this catalog actually are. It is now clear that there are some problems specific to certain situations in the catalog.

GAIA – another ESA project, to be launched in 2013, collecting area 30 $\times$ that of Hipparcos, position measurements 200 $\times$ more accurate than Hipparcos.

SIM (space interferometry mission) – JPL project, very ambitious project, very technically challenging, very high accuracy astrometry, search for planets, goal is to measure positions for stars with $V < 15$ mag to an accuracy of 4×10^{-6} arcsec, with many measurements of the each star. This will yield parallaxes for distances of up to 10^5 pc (100

kpc), which includes the entire Milky Way Galaxy. SIM can measure proper motions and parallaxes for the entire galaxy ! JPL completed the technology development to enable SIM, but the proposed mission turned out to be very expensive and very complex, and in 2010, NASA decided not to proceed with it.

Parallax Projects

Either on the ground or in space, a parallax project must observe a star repeatedly over a year (probably over several years) to measure a parallax.

The project must have a list of stars to be observed BEFORE the project can begin (an input catalog).

There must be a scheduling algorithm (minimize telescope moves, dead time, maximum coverge at the right time of the year for an object, etc).

There must be ongoing monitoring of the whole survey for quality.

After enough measurements have accumulated, data analysis for π values for each star in the input catalog.

Instrument and telescope must be DEDICATED, and cannot be shared. The precision required is so difficult to achieve that one can't afford any changes to setups, spatial scales, etc over the entire observational phase of the survey.

Problem: the reference frame of non-moving (fixed) objects. To do the analysis one needs a set of objects at infinite distance that are not moving against which motions of nearby objects can be measured.

Galaxies are too big.

QSOs are OK (most of the time), but they are rare, and they are much fainter than the survey objects.

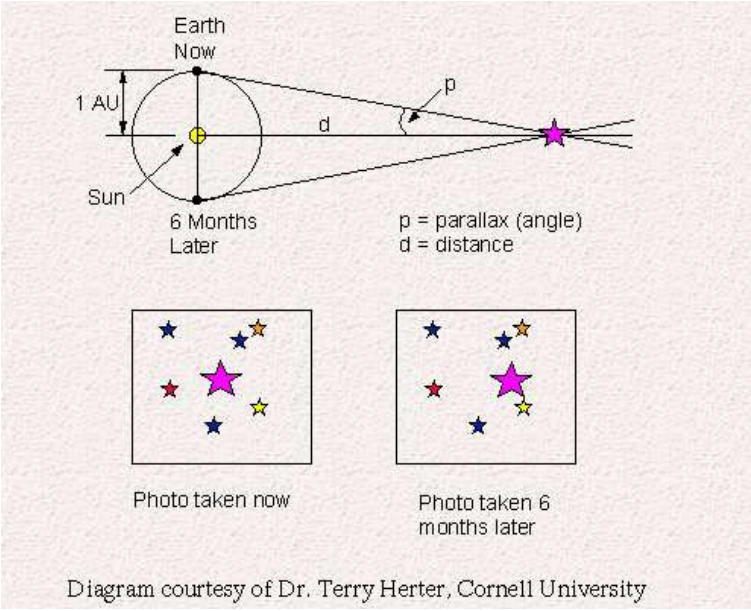

Fig. 2.— Top: the definition of parallax. The bottom panel illustrates the movement of a nearby star as compared to the background of faint distant stars.

Mass and Radius Measurements for Stars

Masses

The mass of the Sun can be determined if one knows the radius of the Earth's orbit around the Sun and assumes $M(Earth) << M_\odot$, and the orbit of the Earth around the Sun is approximately circular.

Newton's law: $GM(Earth)M_\odot/r^2 = M(Earth)v^2/r$. If r is known, then v (the orbital velocity) is known ($v = 2\pi r/P$, P is the period, 1 year). This gives $M_\odot = 1.99 \times 10^{33}$ gm.

All other stellar masses are from binaries except for a few gravitational redshifts for white dwarfs. The problems of binaries are: we only see the orbit projected onto the sky, not the full 3D orbit, and we do not know the inclination angle, the angle that the orbital plane makes with the plane of the sky.

Also for binary stars, the assumption that $M_2 << M_1$ is rarely valid. (The convention is that the most massive component of a binary is star 1.) This means that the stars in the system orbit around the center of mass which may not be in or even close to the M_1, unlike the planet case, where the center of mass is within, and close to the center, of the Sun.

Visual Binaries, the orbit of each star is an ellipse about the center of mass of the system, a circle when the ellipticity is 0. Let a_1 and axis of each orbit (the radius for circular orbits). Then we define a as $a_1 + a_2$. Assume the parallax π of the system is known. Then for an orbital separation between star 1 and 2 on the sky, θ, $a/1$ AU $= \theta/\pi$ and Newton's law becomes

$$M_1 + M_2 = \frac{4\pi^2 a^3}{P^2 G}$$

or $(M_1 + M_2)/M_\odot = (\theta^3/\pi^3)(1\mathrm{yr}/P)^2$.

Consider the typical accuracy of the data: $\pi = 0.050 \pm 0.05$", so 10% for π, same for a. This leads to a large ($\approx$30%) error in $M_1 + M_2$.

How can we separate M_1 and M_2 to complete the solution ? We need v_r amplitudes or proper motion undulations of the two stars. The former requires a double lined spectroscopic binary, period P, radial velocity amplitudes of k_1 and k_2, in km/sec. The latter requires a binary close enough to detect the proper motion undulations of each of the component stars.

Then set q to be the ratio of the masses $q = M_1/M_2 = k_2/k_1$. q is a measured quantity for a double lined spec. binary. $1 + 1/q = (M_2 + M_1)/M_1$, and $1 + q = (M_2 + M_1)/M_2$. For proper motion undulations, $q = M_1/M_2 = \mu_2/\mu_1$.

Let i be the angle of inclination of the orbit plane to the line of sight. Then $P = 2\pi r/v = 2\pi r_2/(k_2/sin(i)) = 2\pi r_1/(k_1/sin(i))$

This provides the necessary separation, i.e.

$$r_1 = \frac{M_2}{(M_1 + M_2)}a = \frac{a}{(1+q)}, \quad r_2 = \frac{a}{(1+1/q)}$$

Combining the above we get

$$G(M_1 + M_2) = \frac{4\pi^2 a^3}{P^2} = \frac{4\pi^2}{P^2}[(1+1/q)r_2]^3 = (\frac{P}{2\pi})(\frac{k_2^3}{sin^3 i})(1+1/q)^3$$

So we finally have the separate equations:

$$(sin^3 i)M_1(1+1/q)G = \frac{P}{2\pi}k_2^3(1+1/q)^3$$

and

$$(sin^3 i)M_2(1+q)G = \frac{P}{2\pi}k_1^3(1+q)^3$$

.

With these two equations and the one for the sum of the masses of the two components, we can now solve for M_1 and M_2 separately.

The inclination of a binary system is unknown. Lets look at some mean values, assuming a random orientation of the orbital plane with respect to the plane of the sky. Let $\theta = 90 - i$. Then

$$< sin(i) >= \frac{\int_0^{2\pi} \int_0^{\pi/2} sin(90-\theta) cos\theta d\theta d\phi}{\int \int cos\theta d\theta d\phi} = \frac{2\pi \int_0^{\pi/2} cos^2\theta d\theta}{2\pi}$$

Since $< cos^2\theta >= 1/2, < sin(i) >= \pi/4$. But we need $< sin^3(i) >$, which is $\int_0^{\pi/2} cos^4\theta d\theta$. Using a table of definite integrals, this is evaluated as $3\pi/16$. So now

$$G < (M_1 + M_2) >= (\frac{P}{2\pi}) \frac{k_2^3 (1 + 1/q)^3}{(3\pi/16)}$$

.

Eclipsing Binaries

In this case, the inclination of the orbit is known, i.e. the plane of the orbit is, to within a few degrees, perpendicular to the plane of the sky ($i \approx 90°$). Of course, this means that only a small fraction of spectroscopic binaries are eclipsing binaries.

For a system with $i = 90°$, one of the two eclipses is a total eclipse, and the light curve has a flat bottom during that eclipse.

If i is not close enough to 90°, the eclipses are partial, as shown in the figure.

Given i, we can solve for the two masses individually, M_1 and M_2.

The range of masses found for stars is from $\sim 0.1 M_\odot$(Ross 614B) to 60 $M_\odot$(Plaskett's star), with a maximum near 120 $M_\odot$(HD 93129A). We can understand the lower mass

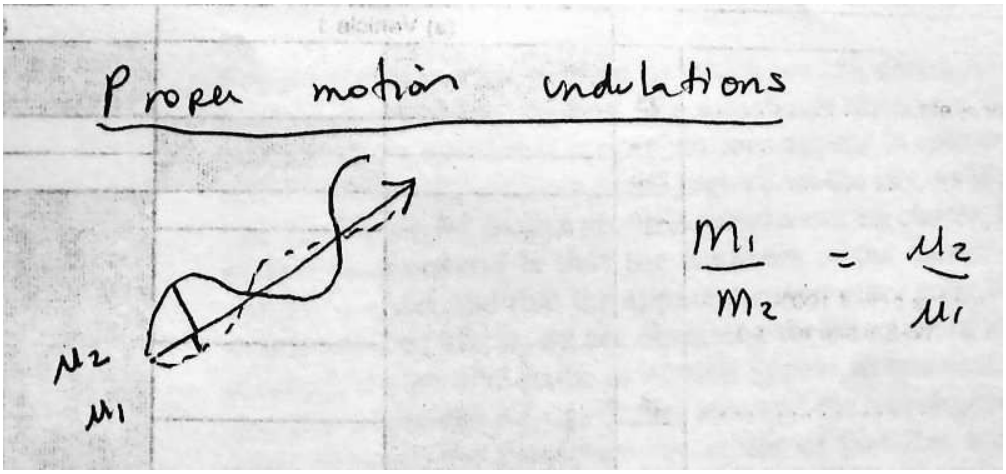

Fig. 4.— Sketch of proper motion undulations due to orbital motion in a binary star system.

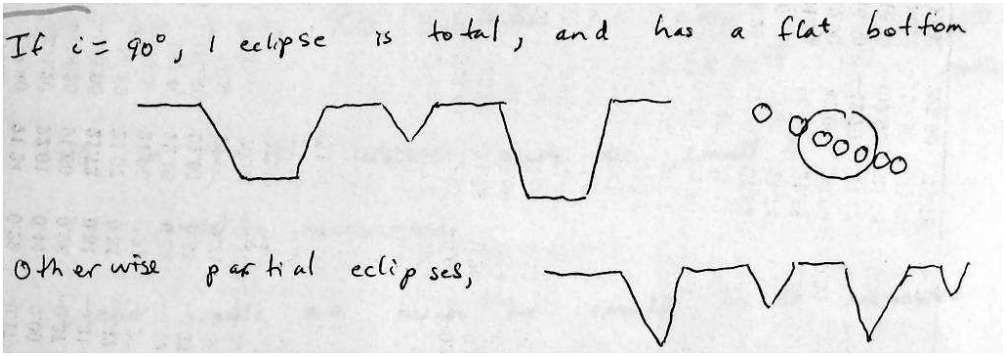

Fig. 5.— The light curve of an eclipsing binary with total eclipses ($i = 90°$) and with partial eclipses (i not exactly $90°$.

limit, the center of the star is too cool for thermonuclear reactions to ever ignite efficiently, at lower masses than this limit, stars are called "brown dwarfs". We will see that the upper mass limit is related to pulsational instabilities brought on by the very high radiation pressure in such luminous stars.

Movie: simulation of orbiting binary stars by Terry Herter of Cornell, http://instruct1.cit.cornell.edu/courses/astro101/java/binary/binary.htm.

Of course, there are triple systems as well !

Searching for Planets

A Jupiter around a Sun at at distance of 10 pc would produce an astrometric wobble with an amplitude of 0.5 milliarcsec (mas), while an Earth-like planet would have a wobble of only 0.3 mas. This is very small and impossible to measure without use of interferometry in space. The figure below, from planetquest.jpl.nasa.gov/science/finding_planets.cfm, shows the result from a model for the entire Solar system, including perturbations from Saturn and other planets of the astrometric displacement of the Sun due to Jupiter.

Photometric search - look for transits, light of star + planet becomes light of star only, small drop in flux (about 1%) is hard to measure from the ground, easier with HST, see Brown et al, 2001, ApJ, 552, 699. Maximum drop in flux for planet of HD 209458 is 1.5% of continuum, $R_p = 1.35 \pm 0.06\ R_J$, $i = 86.68 \pm 0.14$ deg, $R(star) = 1.146 \pm 0.050 R_\odot$. If the photometric light curve reveals transits amd a radial velocity curve for the orbit exists, the radius of the planet can be derived, and since the mass of the planet is known from the orbit, ρ can be obtained, which constrains the composition of the planet.

Detection of planet transits is now "routine" with the Kepler satellite, launched March 6, 2009 with a 3.5 year mission lifetime. It continuously monitors a single 115 square degree field. Photometric precision is $\sim$50 parts/million for a G2V star with V 12 and

DOPPLER - WOBBLE TUTORIAL

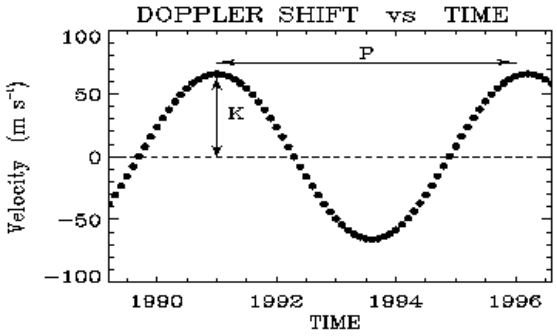

Kepler:

$$r^3 = \frac{GM_*}{4\pi^2} P^2$$

Observe Period.

$$V_{\rm PL} = \sqrt{GM_*/r}$$

–> Vel. of Planet .

Momentum Conservation:

$$M_{\rm PL} = M_* V_* / V_{\rm PL}$$

Observe K $= V_* \sin i$

$$==> \; M_{\rm PL} \sin i$$

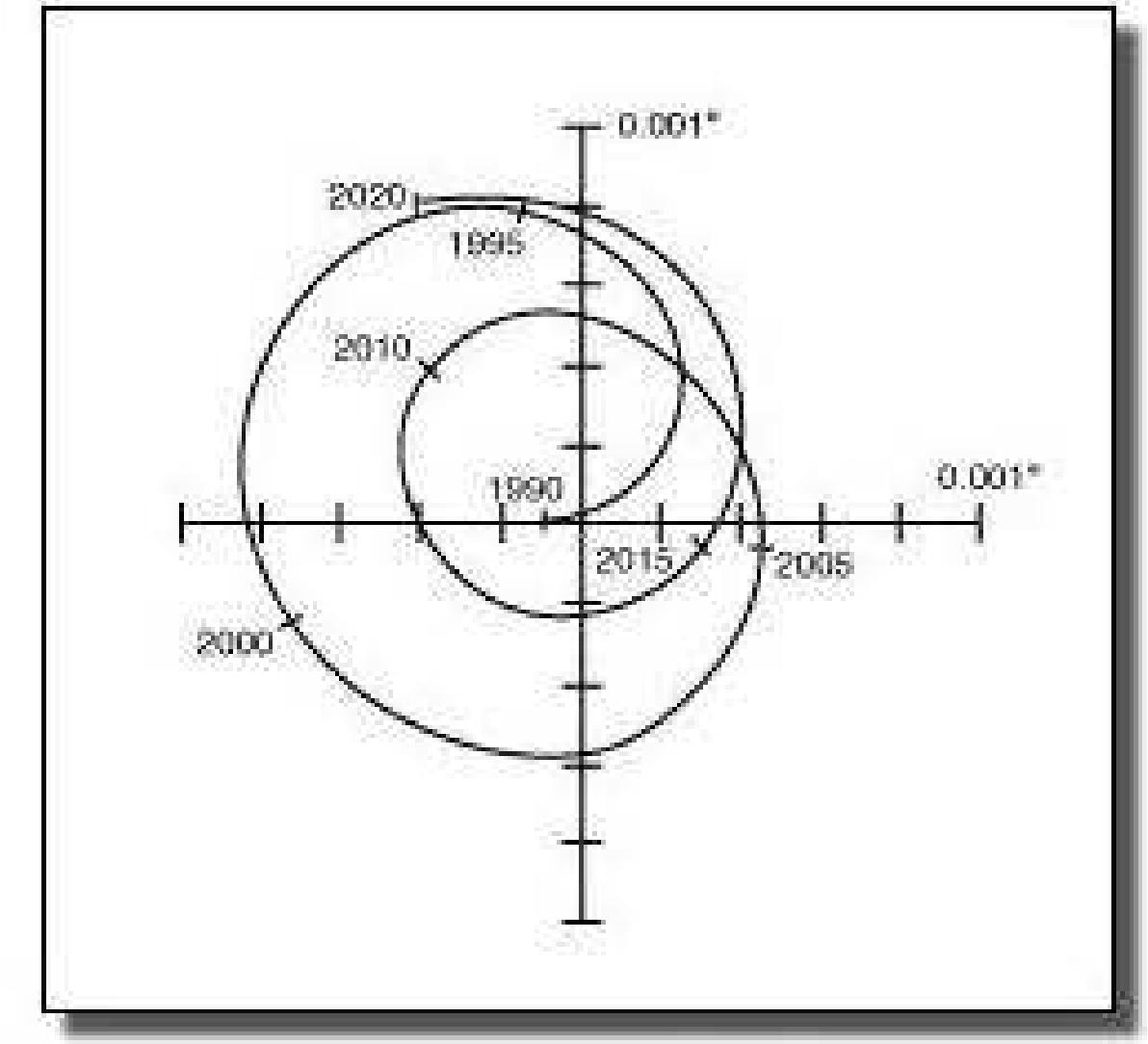

Astrometric displacement of the Sun due to Jupiter as at it would be observed from 10 parsecs, or about 33 light–years.

a 30 min. integration. Such high precision means that many subtle effects, previously neglected, that may influence the light curve of a star – planet system, may be detected which can provide important additional constraints on the system. These effects fall into 3 categories, relativistic beaming of the light, reflection off the surface of the planet, which will vary with the orientation of the illuminated part of the planet with repected to the line of sight, and ellipsoidal effects if a member of the binary system is tidally affected by the gravitational force of its companion and becomes non-spherical. The first of these, rotational doppler beaming, is the photometric equivalent of the Rossiter-McLaughlin effect seen in radial velocities of spectral lines during ingress and egress of an eclipse/transit) (see Groot, arXiv:1104.3428, and Shporer, Kaplan, Steinfadt et al, 2010, ApJL) and is by far the largest of these three in both stellar binary and star/planet systems.

Radial velocity searches, which have been the most productive thus far, depend on the v_r accuracy that can be achieved. This is now at or slightly better than 1 m/sec, a phenomenal technical achievement. See the latest result from HARPS group at ESO, for example Pepe et al (2011, arXiv:1108.3473). At this level of precision, stellar pulsation, granulation, convection, magnetic activity cycles etc become major concerns, and the stellar sample under study must consist of "quiet" stars. (see, e.g. Lovis, Dumusque, Santos et al, arXiv:1107.5325 for a discussion of these issues).

Information on statistical properties of the ∼640 (as of Sep. 2012) exo-planets found thus far , see http://exoplanets.org for mass, distance from star, and eccentricity distributions, as well as discussions of the fraction of stars with planets, and why this might depend on metallicity of the star, etc.

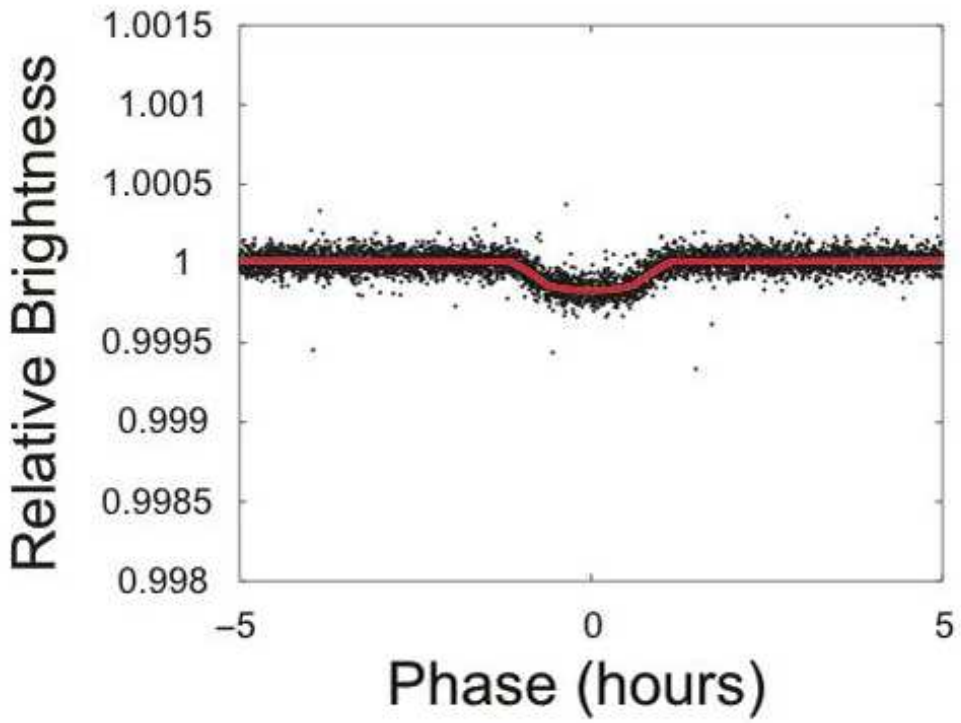

Fig. 7.— The transit light curve of planet Kepler-10b, Kepler's first rocky planet with $M = 4.6M_E, R = 1.4R_E$, and period 0.837 days. Note that the maximum drop in the total light is only 0.05%. This light curve is a tribute to the very high accuracy of the Kepler satellite photometry.

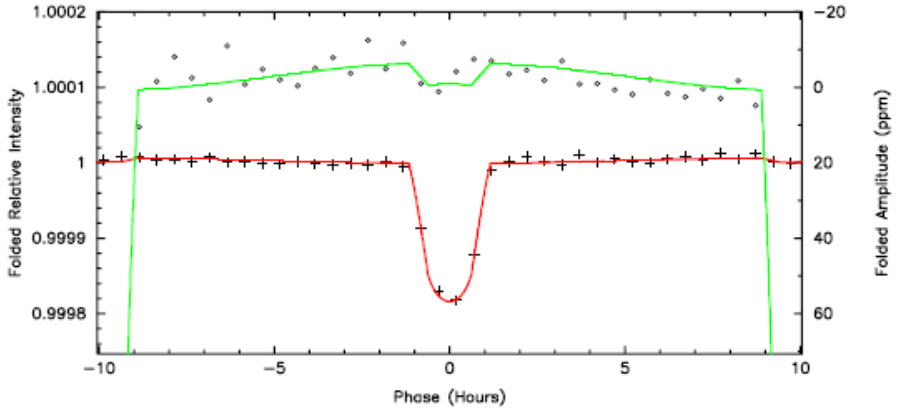

Fig. 13.— The relative intensity scale of the phase-folded light curve of Kepler-10b shown in the bottom panel of Figure 12 is expanded to show the phase modulation and marginal occultation required by the model fits. Colors have the same meaning as in Figure 12.

Fig. 8.— A blown up transit light curve of planet Kepler-10b, showing light curve details at the level of parts/million.

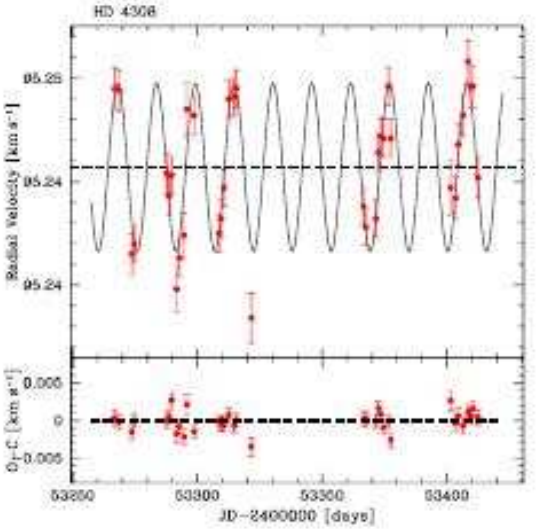

Fig. 5. Intermediate season of HARPS radial velocities for HD 4308. The best Keplerian fit to the data (solid curve) gives a minimum mass of 14.1 $M_\oplus$ and an orbital period of 15.56 days for the planet.

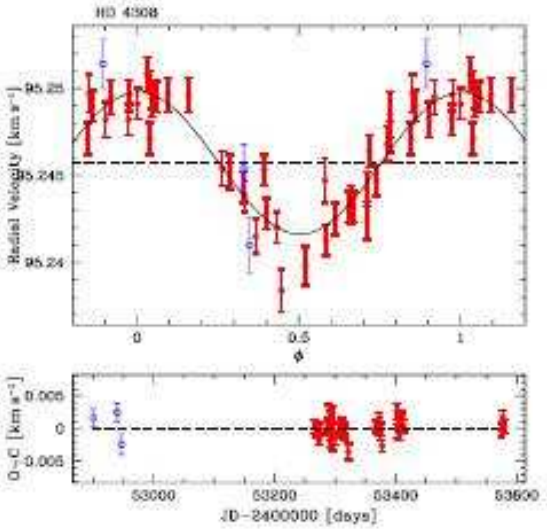

Fig. 6. Phase-folded radial velocities of HD 4308 superimposed on the best Keplerian orbital solution (solid curve). The 3 older points obtained before introducting the new observing strategy (see text) are indicated by open symbols.

Stellar Radii

$R_\odot$= 6.95 $\times 10^{10}$ cm. At $d = 1$ pc, $R_\odot$ subtends an angle of 2.2×10^{-8} radians, which is 4×10^{-4} arcsec, much too small to be directly measured, even with a telescope in space.

Eclipsing binaries offer a way to measure stellar radii through their light curves. The entrance and egress times in the light curve sketched below corresponding to the 4 points marked in the figure are known, and

$$\frac{t_4 - t_1}{P} = \frac{2(R_1 + R_2)}{2\pi a}, \qquad \frac{t_3 - t_2}{P} = \frac{2(R_1 - R_2)}{2\pi a}.$$

A more careful treatment allows for the details of the variation of the illumination across the surface of each star and the gravitational distortions from spherical shape of each star.

Using model atmospheres and limb darkening and multi-color photometry of such a system, we can also derive $T_{\rm eff}$ for each of the component stars throughout the period.

Existing interferometers are now good enough that for the nearest and largest stars, some resolution across the stellar surface is possible, and limb darkening can be directly measured.

Direct radius measurements are only possible with interferometry (see brief description below) and only for the nearest and largest stars.

Lunar occultations (a form of interferometry using the limb of the moon as a star is occulted can be used to measure stellar radi. The main problem with this technique is that the orbit of the moon is fixed and only covers a small part of the 4π steradian of the sky. Also the stars must be very bright so as to get enough signal in the short crucial time when the moon occults the star, so its actual applicability is limited.

Astronomical Units

mag(nitude) = −2.5log10(flux), with 0 mag defined by Vega. Apparent mag ≡ flux received at Earth (varies with distance of object), absolute mag ≡ flux at a fixed distance of 10 pc. Notation convention: M for abs. mag and m for apparent mag, do not confuse with mass !

F(at Earth)/F(10 pc) = (10 pc)$^2/D^2$, so $M = m - 5\log(D) + 5$.

A logarithmic scale is useful because of the large range in F(at the Earth), ranging over many powers of 10. The mag scale is logarithmic, but 1 mag is a factor of 2.5, not 10. Also its backward, brighter objects have more negative mag values.

This is all historic, and has to do with ancient Greeks and Romans and the response of the human eye.

In an ideal world, the mag system would no longer be used, and we'd all switch to Janskys (the cgs flux unit). We should try to avoid using them, but they are so ingrained in the consciousness of older optical astronomers...

Imagine a change in flux F of a factor of $\delta = 10^{-3}F$. This, expresed in mags, is 2.5 Log$[F + \Delta)/F] = log(1 + \Delta) \approx 2.5$ ln(1+δ)/$ln(10) \approx 2.303\delta/2.5 \approx \delta$. So for small flux changes, the change in flux ratio is the same as the difference in millimag.

Bolometric mag: total luminosity, not mag at a particular wavelength, $M_{bol} = -2.5log(L/L_\odot) + M_{bol}$(Sun) $= m_{bol} - 5log(d/10$ pc). M_{bol}(Sun) = 4.74 mag. The term $M_{bol} - M_\lambda$, where λ is the wavelength of interest/observation, is called the bolometric correction.

Flux is measured in real life through a particular filter with transmission T over a particular wavelength regime, so $F \propto \int F_\nu T_\nu d\nu$. T_ν is generally peaked at a particular wavelength/freq., which is the effective λ for that filter/instrument combination. (In real

life, λ_{eff} will depend on the spectral energy distribution of the star, and may be perceptibly different for red vs blue stars...)

Interstellar absorption perturbs the intrinsic stellar spectral energy distribution, reddening it.

Color indices X,Y $\propto log[F(\lambda_{eff}, filterX)/F(\lambda_{eff}, filterY)] = 0.4[m(filterY) - m(filterX)] + A$, A is a constant.

Calibration of the flux in a photometric system is done using observations of some terrestrial source of known flux (a crucible of a melting metal, platinum has been used, or a NIST calibrated standard lamp) mounted on a tower, and observed with a small telescope interleaved with observations of Vega or some other very bright star.

In the center of the optical band, at 500 nm, V = 0.0 mag corresponds to a received flux of 3.8×10^{-9} ergs/sec/cm^2/Å $\equiv$ 1000 photons sec/cm^2/Å (this is Code's number).

1 Jansky = 10^{-23} ergs/cm^2/sec/Hz.

0 mag at 500 nm $\equiv 3.2 \times 10^{-20}$ ergs/cm^2/sec/Hz or 3,200 Jy.

$L_\odot = 3.9 \times 10^{33}$ ergs/sec (emitted luminosity)

$M_{bol} = 0$ mag $\rightarrow L = 3 \times 10^{35}$ erg/sec

$m_{bol} = 0$ mag $\rightarrow F$(at Earth) $= 2.5 \times 10^{-5}$ ergs/cm^2/sec.

Table 1. Traditional Photometric Bands

Name	Central λ (Å)	Full Width Half Maximum (Å)
U(ltraviolet)	3650	680
B(lue)	4400	980
V(isual)	5500	890
R(ed)	7000	2200
I(infrared)	9000	2400
	(microns)	(microns)
J	1.25	0.38
H	1.6	0.4
K	2.2	0.48
L	3.4	0.70
M	5.0	
N	10.2	

Adopted from Allen, Astrophysical Quantities, 3rd edition, section 97. The zero points are also given there.

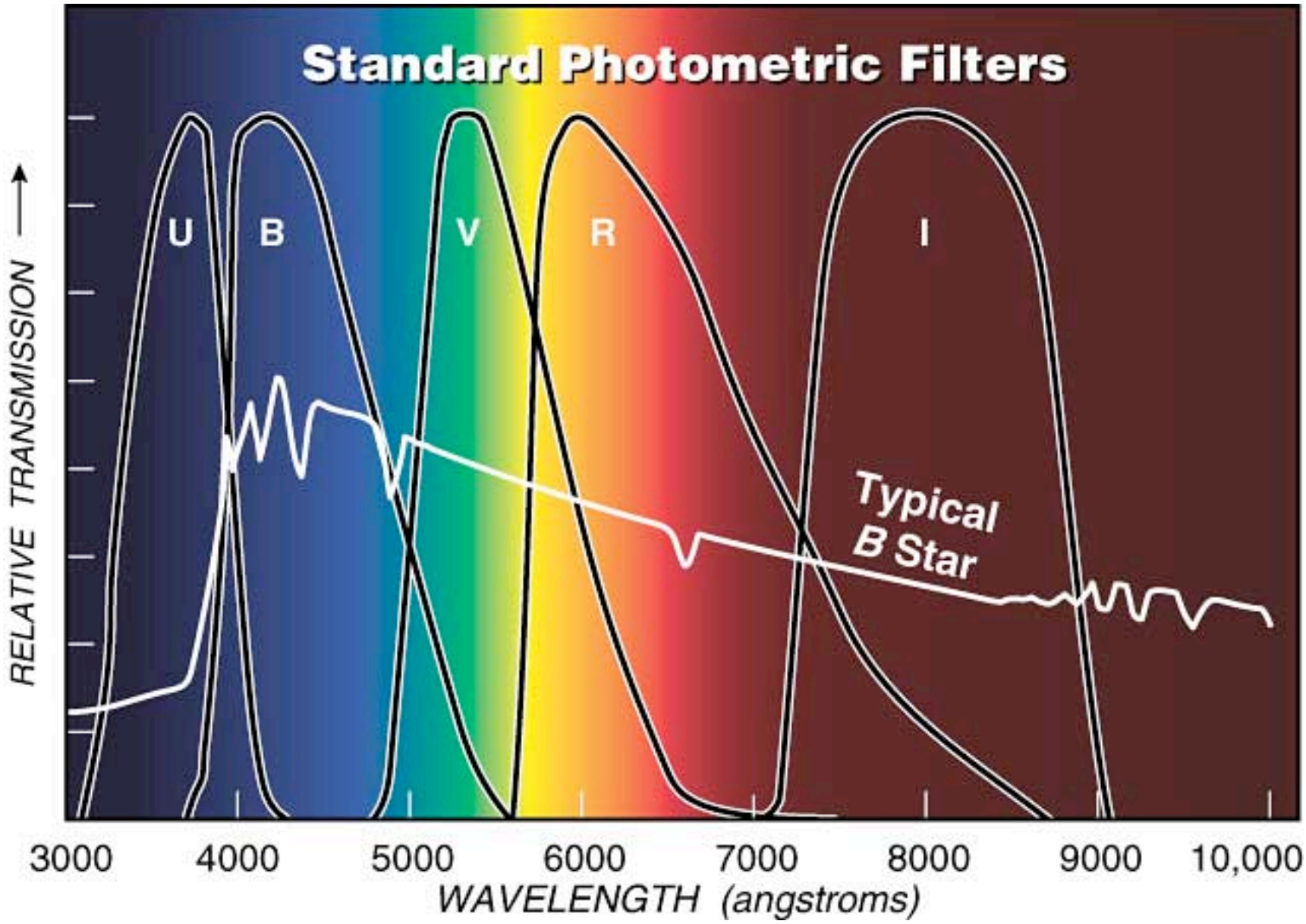

(Sky & Telescope)

Stellar Spectral Classes

Spectral types: these were first devised at Harvard during the development of the Henry Draper catalog. The names of the various spectral types are historical, but the concept is useful, and the classes correspond to different ranges of physical parameters, mostly $T_{\rm eff}$, with the luminosity classes depending on $\log(g)$ as a secondary parameter.

Spectral classification (based on characteristics of stellar absorption lines) (a good indicator of effective temperature) (The luminosity given is for main sequence stars.)

The cooler stars of a given $T_{\rm eff}$ are subdivided in accordance with whether the abundance of C is greater than or less than that of oxygen in their atmospheres. The latter is the normal case; these are M stars, with TiO dominant in the optical regime. C stars (sometimes further broken down into R stars, which are the warmer of these stars, with $T_{\rm eff}$ $\sim$ 4000 K) and N stars, with $T_{\rm eff}$ $\sim$ 3000 K) have C dominant, hence C_2 and CH are very strong, while stars with C and O about equally abundant (S stars) show ZrO bands.

The Sun is a G2V star in this classification scheme.

90% of stars can be satisfactorily classified by the above scheme. The remainder are special cases where rare effects cause the star to appear peculiar, for example peculiar A stars (Ap stars) have strong magnetic fields that inhibit convection and thus have abnormally strong lines of certain elements (Si, Mn, Cr, Sr, Eu...), while very metal poor stars also fail to fit into the above scheme.

Table 2. Stellar Spectral Classes

Name	$T_{\rm eff}$ (1000 K)	$\log[L/L_\odot]$	Dominant Features
O	> 25	> 5	HeII
B	11–25	2–5	HeI, Balmer HI
A	7.5–11	2–5	Balmer lines dominant
F	6–7.5	0–1	CaII, Fe I, ionized metals
G	5–6	$-0.3 - 0$	CH, CN, neutral metals, CaII, FeI
K	3.5–5	$-1 - -0.3$	molecular bands, metals
M	2.5–3.5	< -1	TiO
C			Carbon rich variant of M, CH, CN, C2
L	2.0		Water
T	1.0		Methane
MK	Luminosity	Classes	(indicates surface gravity)
Ia			Most luminous supergiants
Ib			Luminous supergiants
II			Luminous giants
III			Giant
IV			Subgiant
V			Main sequence dwarf

Luminosity discrimination based largely on line width, higher gravity stars have broader lines.

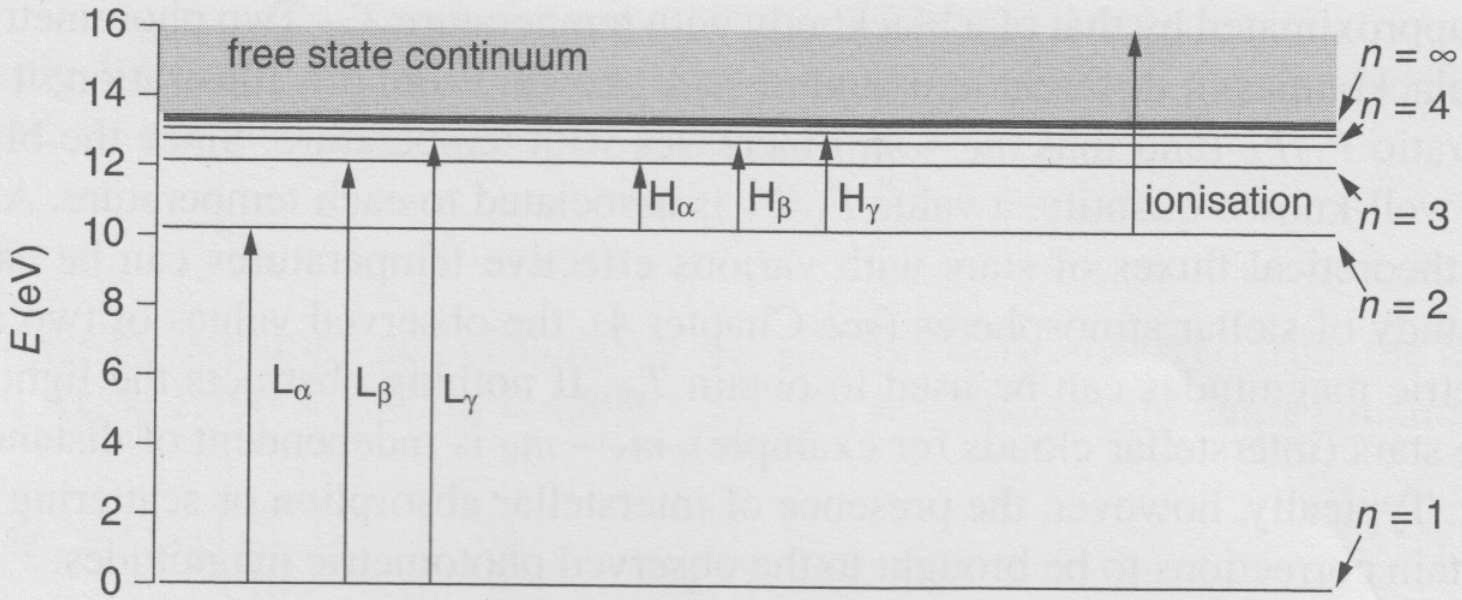

Figure 1.5 Energy levels of hydrogen in eV. Various bound-bound transitions are also shown, as well as a bound–free transition from level $n = 2$ (see Section 1.6 for more details).

LeBlanc – An Introduction to Stellar Astrophysics

Line	Transition	Wavelength
H_α	$3 \rightarrow 2$	6563 Å
H_β	$4 \rightarrow 2$	4861 Å
H_γ	$5 \rightarrow 2$	4341 Å
H_δ	$6 \rightarrow 2$	4102 Å
H_ϵ	$7 \rightarrow 2$	3970 Å
H_ζ	$8 \rightarrow 2$	3889 Å
H_η	$9 \rightarrow 2$	3835 Å
...		
H_∞	$\infty \rightarrow 2$	3646 Å

Balmer emission spectrum (Source: Wikipedia)

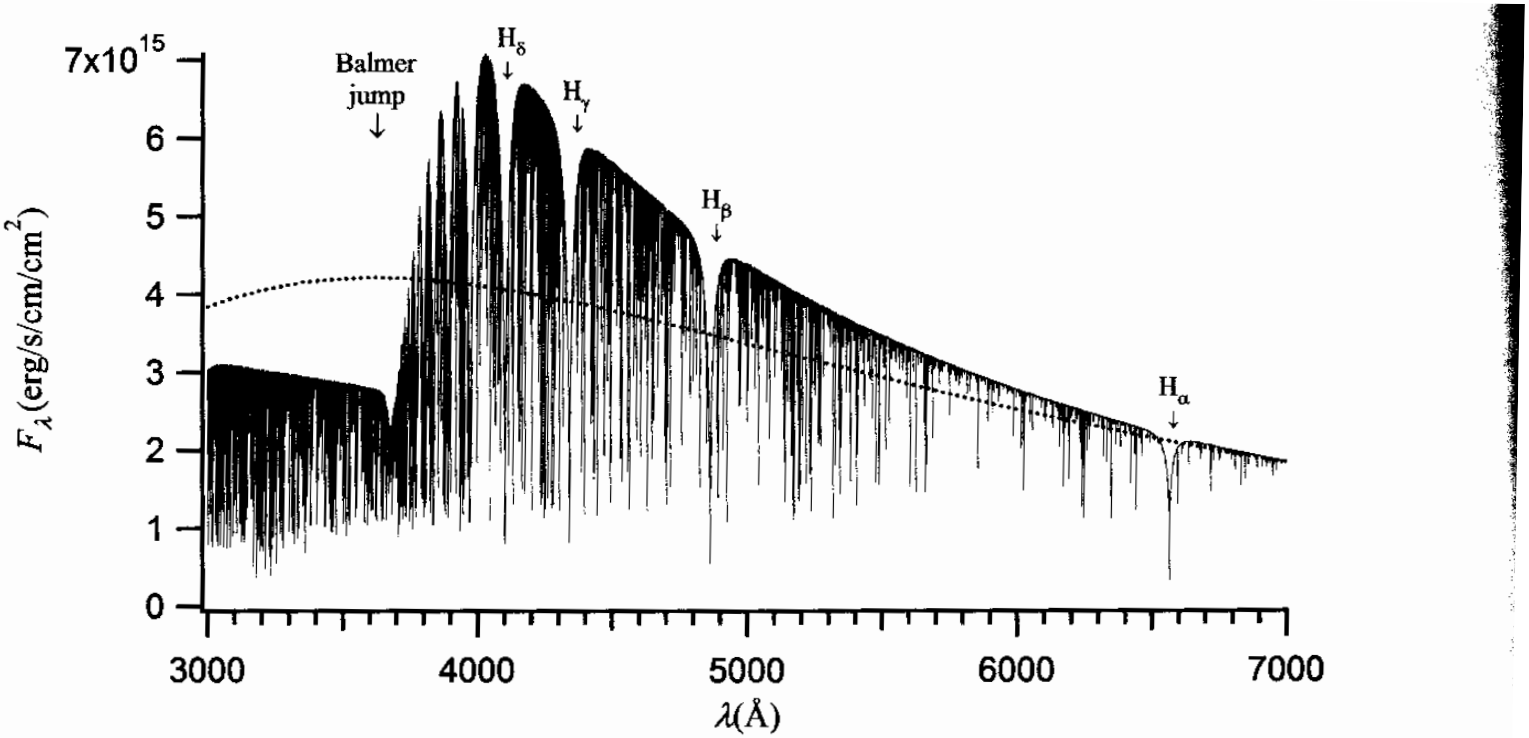

Figure 1.8 Theoretical monochromatic flux emerging form an A type star with $T_{\text{eff}} = 8000\,\text{K}$. The first four Balmer absorption lines, as well as the Balmer jump, are identified in this figure. Thousands of other absorption atomic lines can also be seen. This theoretical flux was obtained with the Phoenix stellar atmosphere code (Hauschildt, P.H., Allard, F. and Baron, E., *The Astrophysical Journal*, **512**, 377 (1999)) while using the elemental abundances found in the Sun. The flux at the surface of a blackbody with $T = 8000\,\text{K}$ (dotted curve) is also shown.

LeBlanc – An Introduction to Stellar Astrophysics

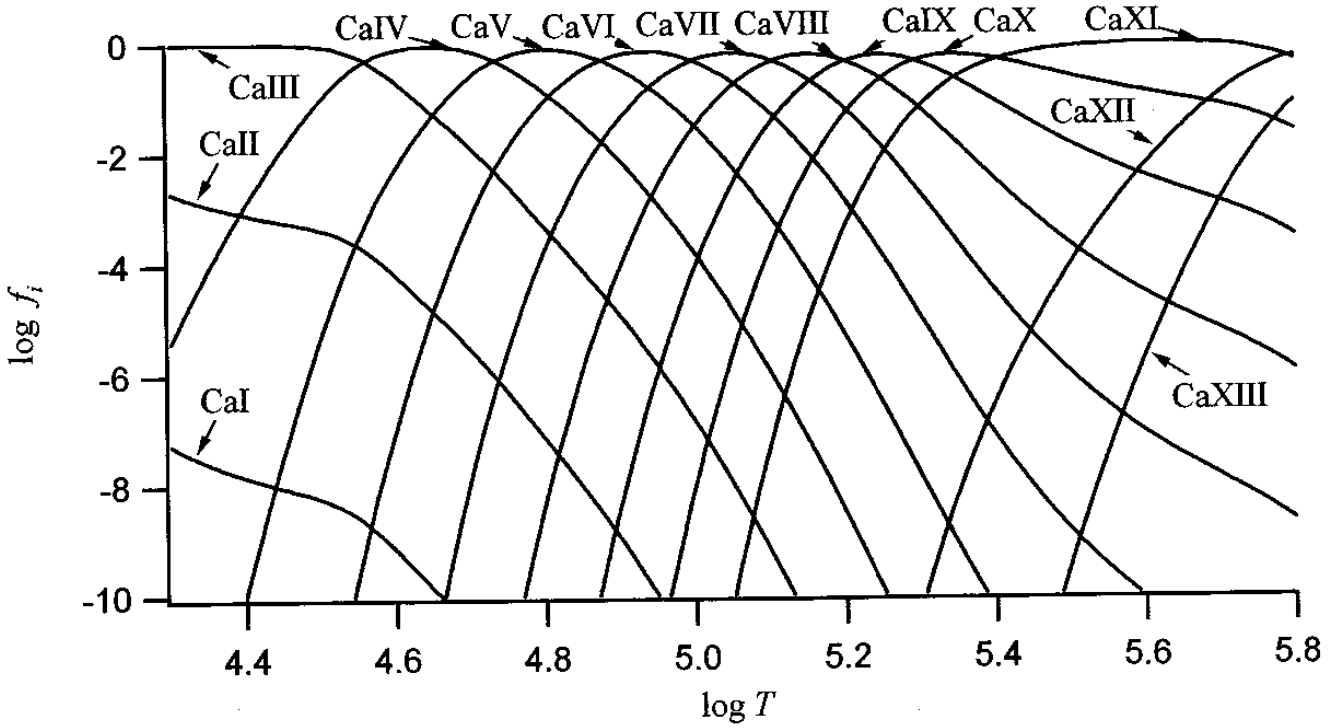

Figure 1.7 Ionisation fractions (f_i) of Ca ions as a function of temperature (or depth) in the interior of a star with $T_{\rm eff}$ = 7600 K. The surface of the star is found at the left side of the horizontal axis.

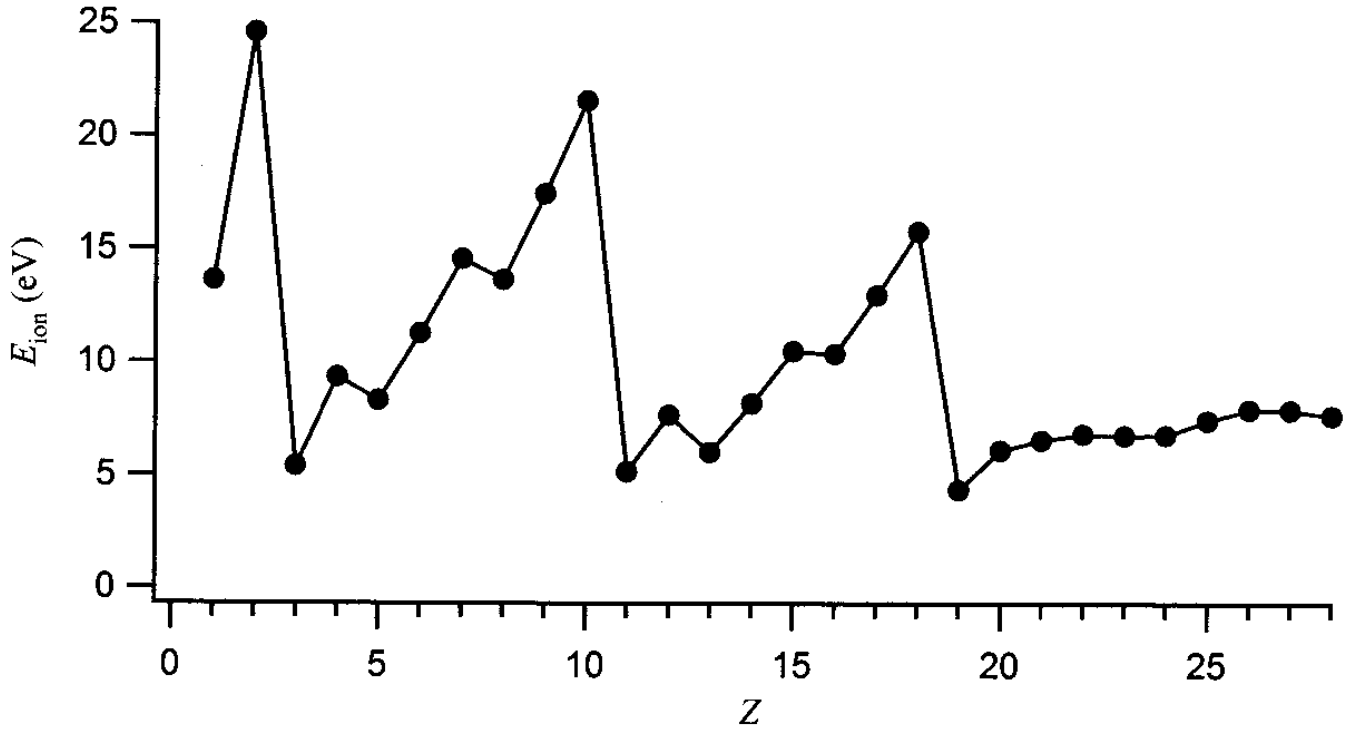

Figure 1.6 Ionisation energy (from the fundamental atomic energy state) as a function of atomic number for neutral atoms.

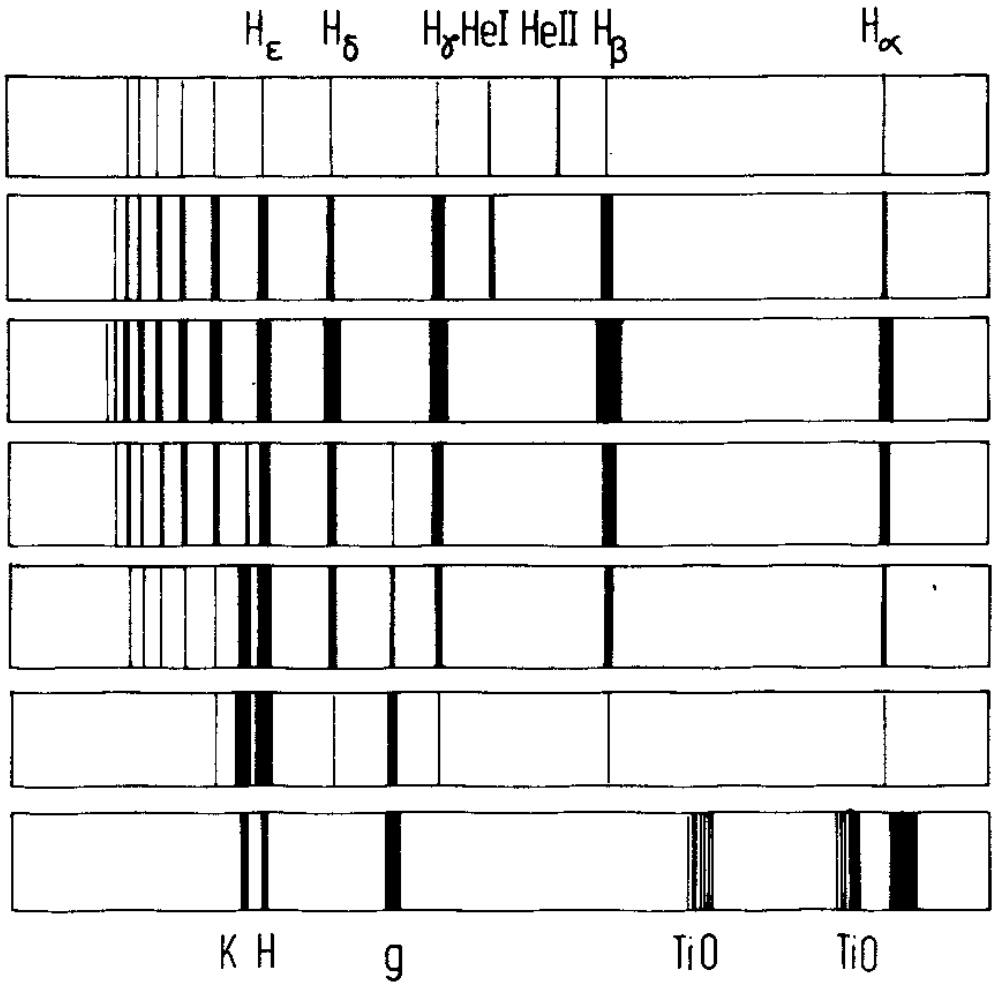

Abb. I.21: Schematische Darstellung der Spektralsequenz.

Scheffler & Elsässer, Physik der Sterne und der Sonne

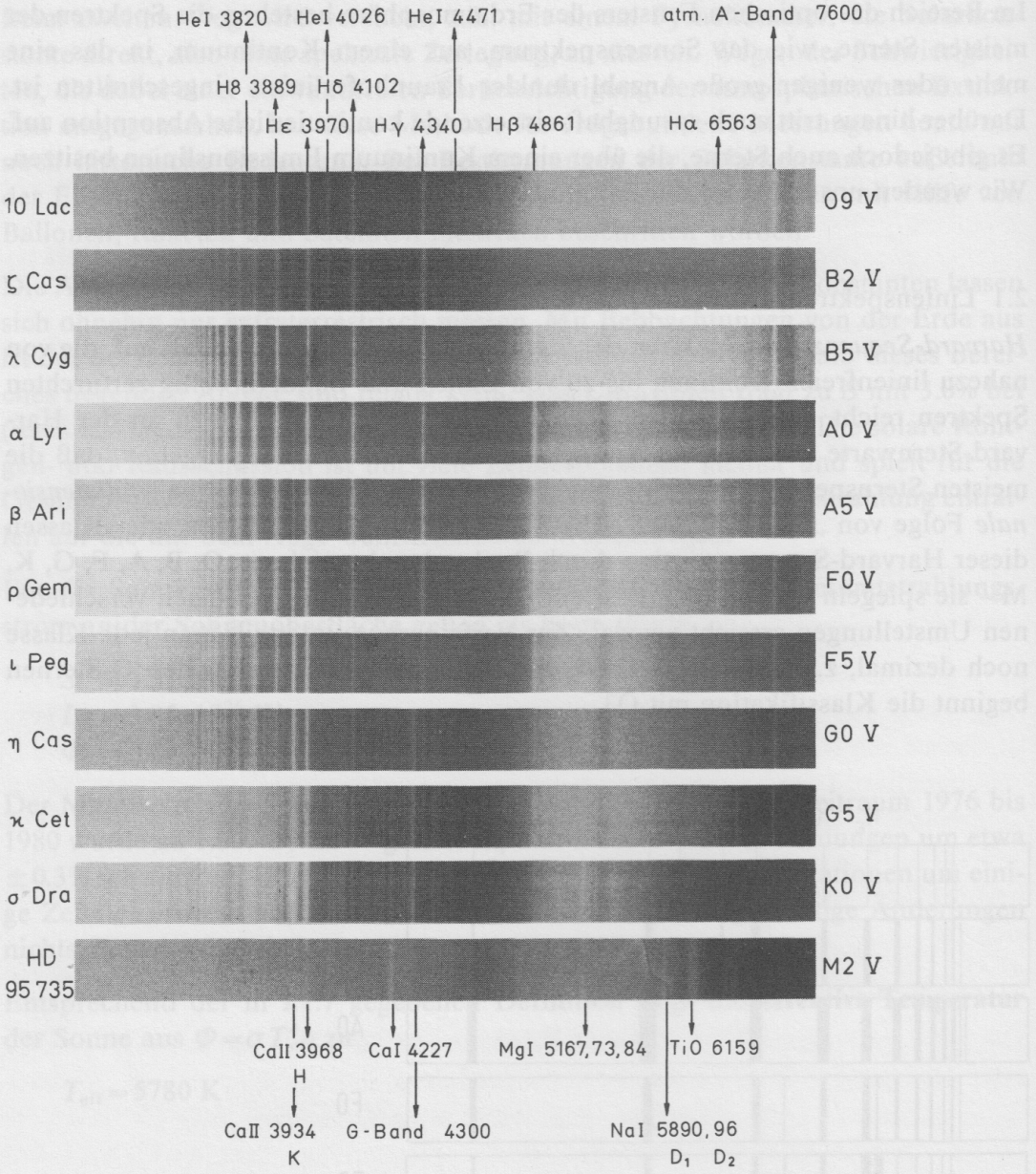

Abb. I.22a: Die Spektralklassen der Hauptreihe (Leuchtkraftklasse V, siehe I.2.10) repräsentiert durch Objektivprismenspektren ausgewählter Sterne (W. Seitter). Die Aufhellungen im Kontinuum zwischen 5000 und 6500 Å ergeben sich durch eine Empfindlichkeitslücke („Grünlücke") des verwendeten Photomaterials.

Scheffler & Elsässer,
Physik der Sterne und der Sonne

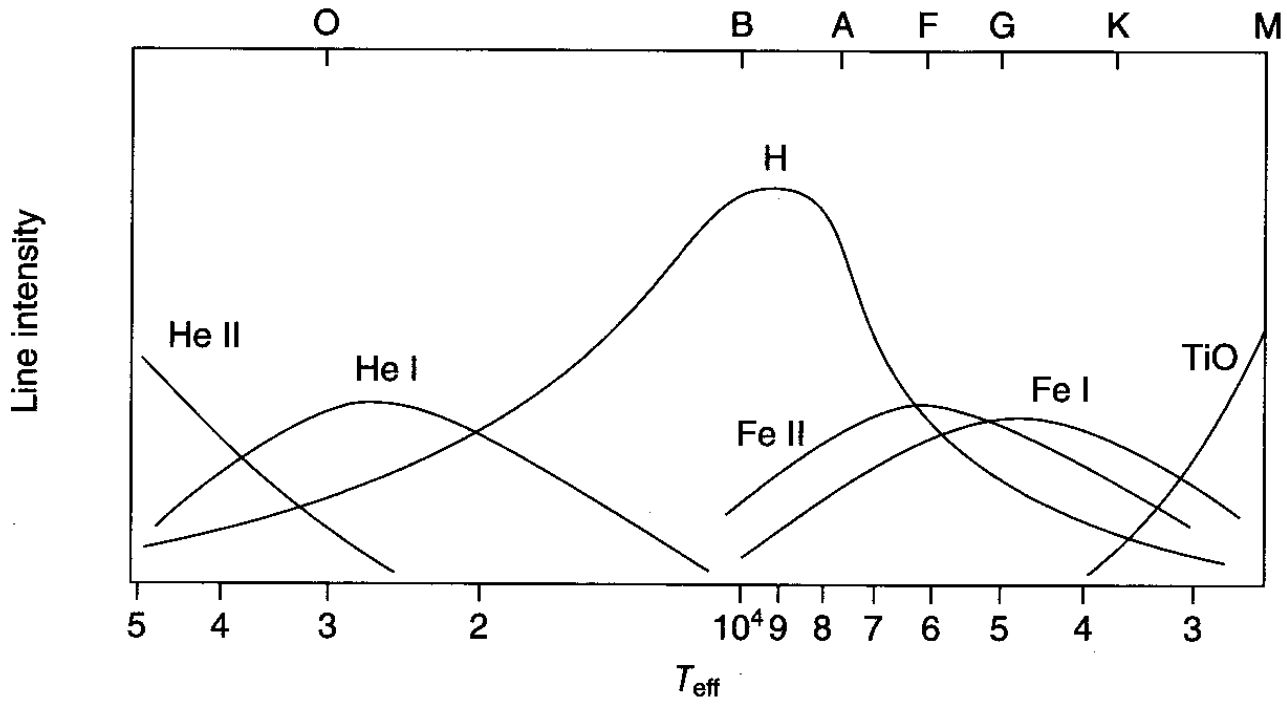

Figure 1.9 Approximate line intensity as a function of T_{eff} for several ions. The spectral types (these are positioned at the coolest temperature for each class) and the intensity of the TiO molecular bands are also shown.

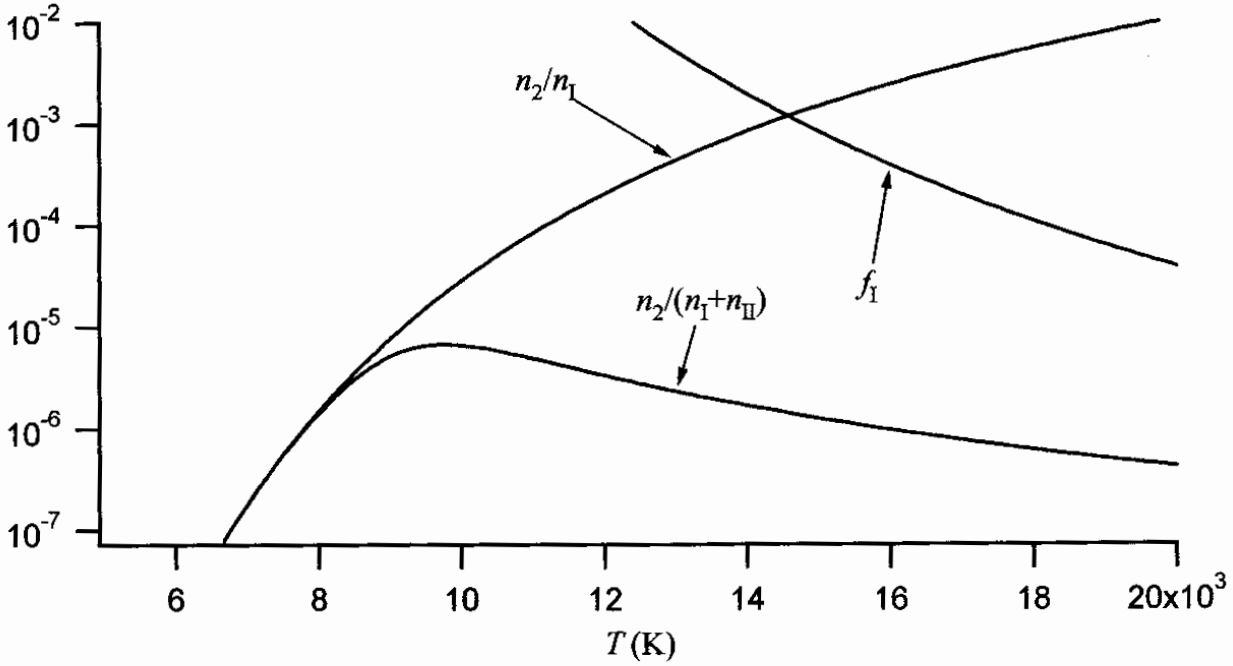

Figure 1.10 Illustration showing the portion of neutral hydrogen atoms found in the $n = 2$ level (n_2/n_I), the neutral ionisation fraction ($f_I = \frac{n_I}{n_I + n_{II}}$) and the product of these two factors that give the portion of all hydrogen atoms found in the $n = 2$ level (i.e. $\frac{n_2}{n_I + n_{II}}$).

Spectral type	T_{eff} (K)	$M/M_{\odot}$	$L/L_{\odot}$	$R/R_{\odot}$
O5	42 000	60	400 000	12
B0	30 000	17.5	40 000	7.4
B5	15 200	5.9	730	3.9
B8	11 400	3.8	140	3.0
A0	9790	2.9	48	2.4
A5	8180	2.0	12	1.7
F0	7300	1.6	5.7	1.5
F5	6650	1.4	3.0	1.3
G0	5940	1.05	1.4	1.1
G5	5560	0.92	0.73	0.92
K0	5150	0.79	0.46	0.85
K5	4410	0.67	0.18	0.72
M0	3840	0.51	0.070	0.60
M2	3520	0.40	0.034	0.50
M5	3170	0.21	0.0066	0.27

LeBlanc – An Introduction to Stellar Astrophysics

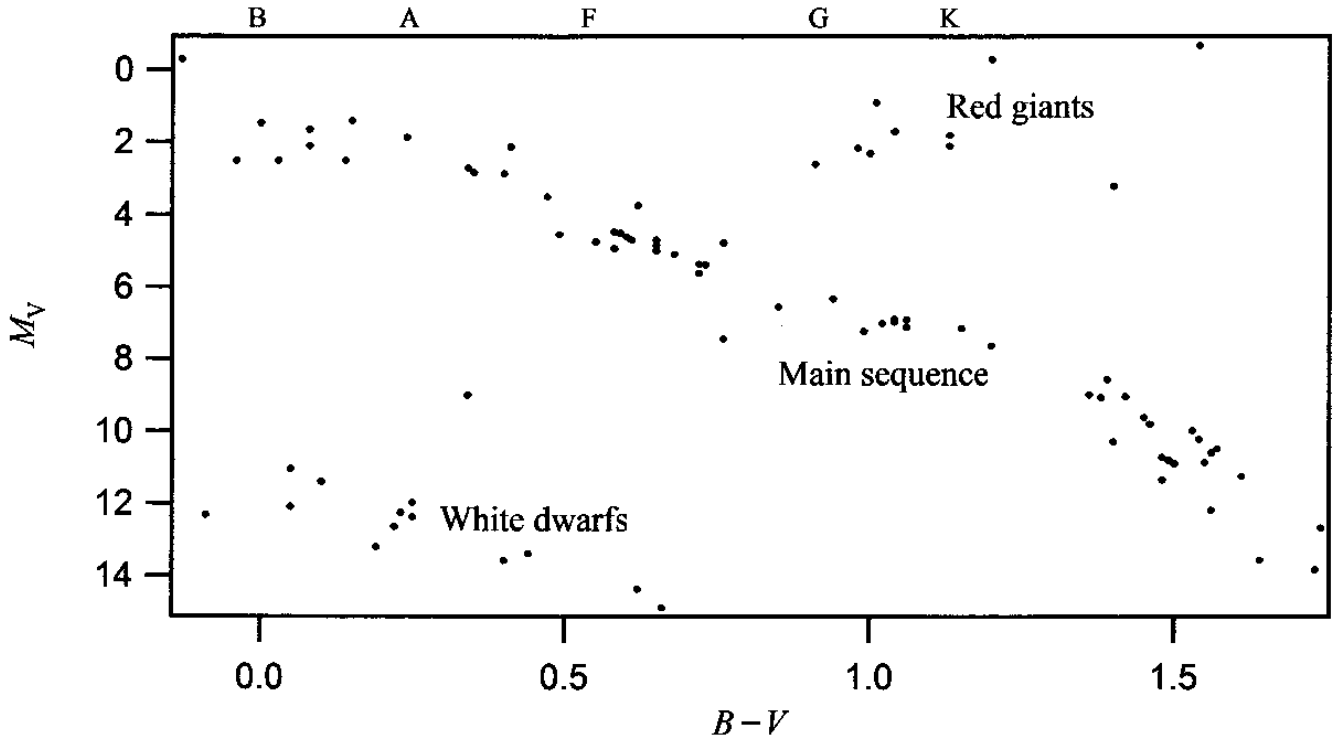

Figure 1.11 A sample taken among the 1000 nearest stars on a color-magnitude H–R diagram. The spectral types are also shown (these are positioned at the coolest temperature for each class).

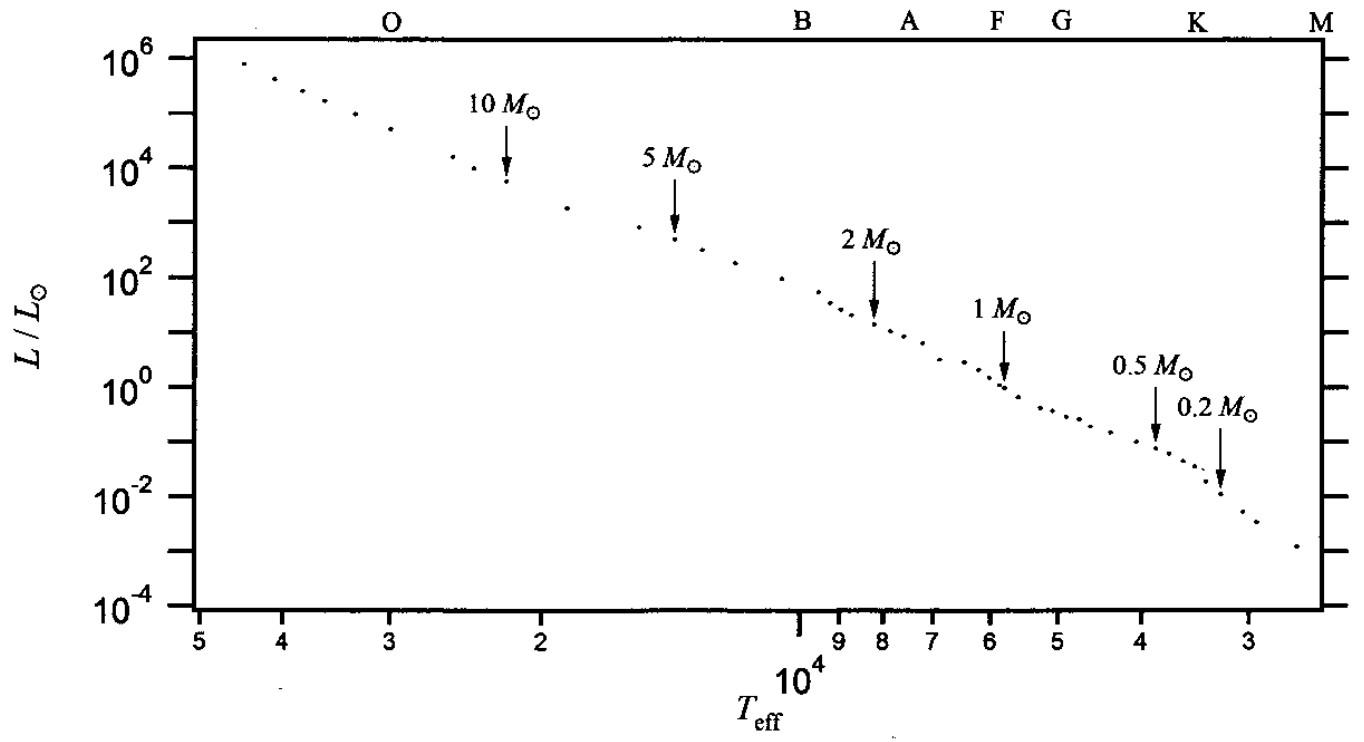

Figure 1.12 The main sequence on an H–R diagram. Several values of the mass are given. The spectral types are also shown (these are positioned at the coolest temperature for each class).

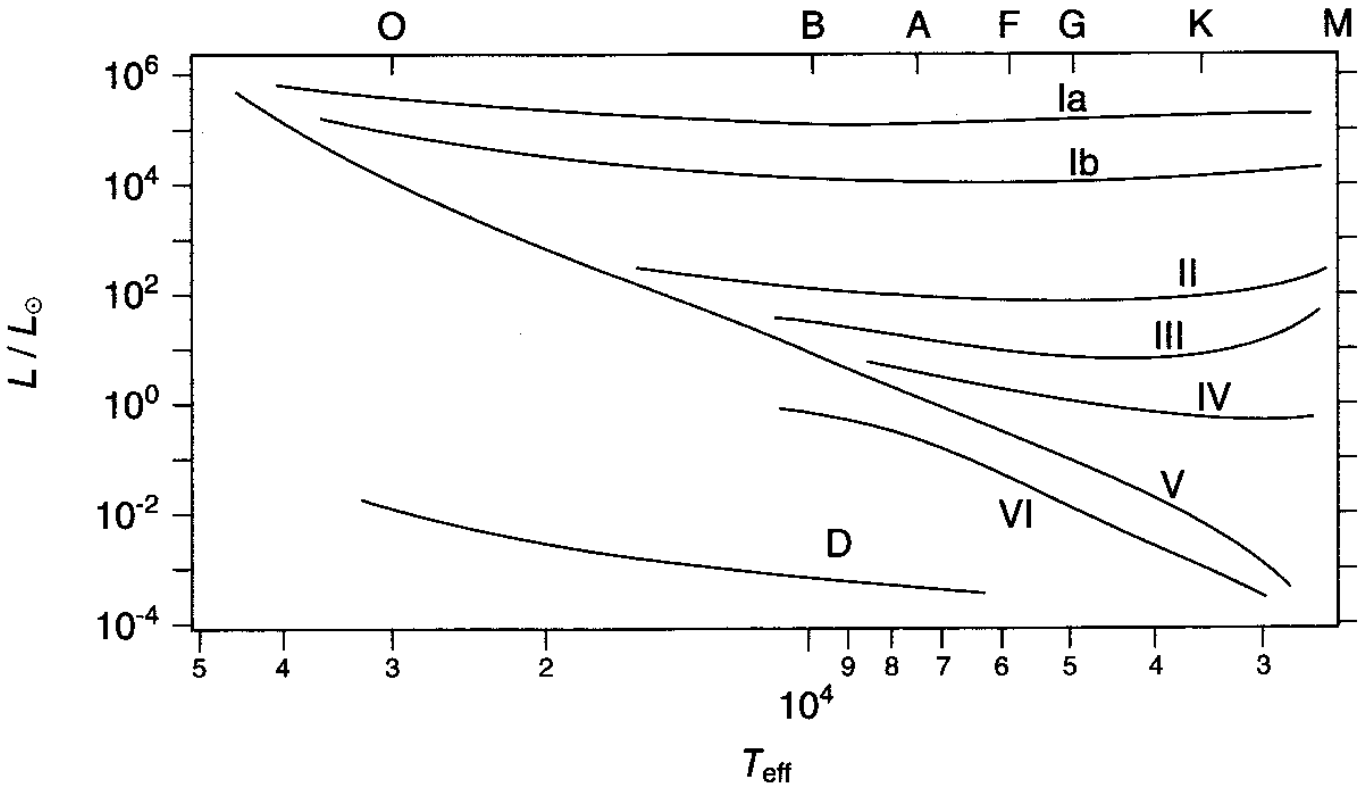

Figure 1.14 Luminosity classes of the H–R diagram. These are identified in Table 1.7. The spectral types are also shown (these are positioned at the coolest temperature for each class).

Table 1.7 Luminosity classes.

Ia	Bright supergiants
Ib	Supergiants
II	Bright giants
III	Giants
IV	Subgiants
V	Main-sequence stars (or dwarfs)
VI (or sd)	Subdwarfs
D (or VII)	White dwarfs

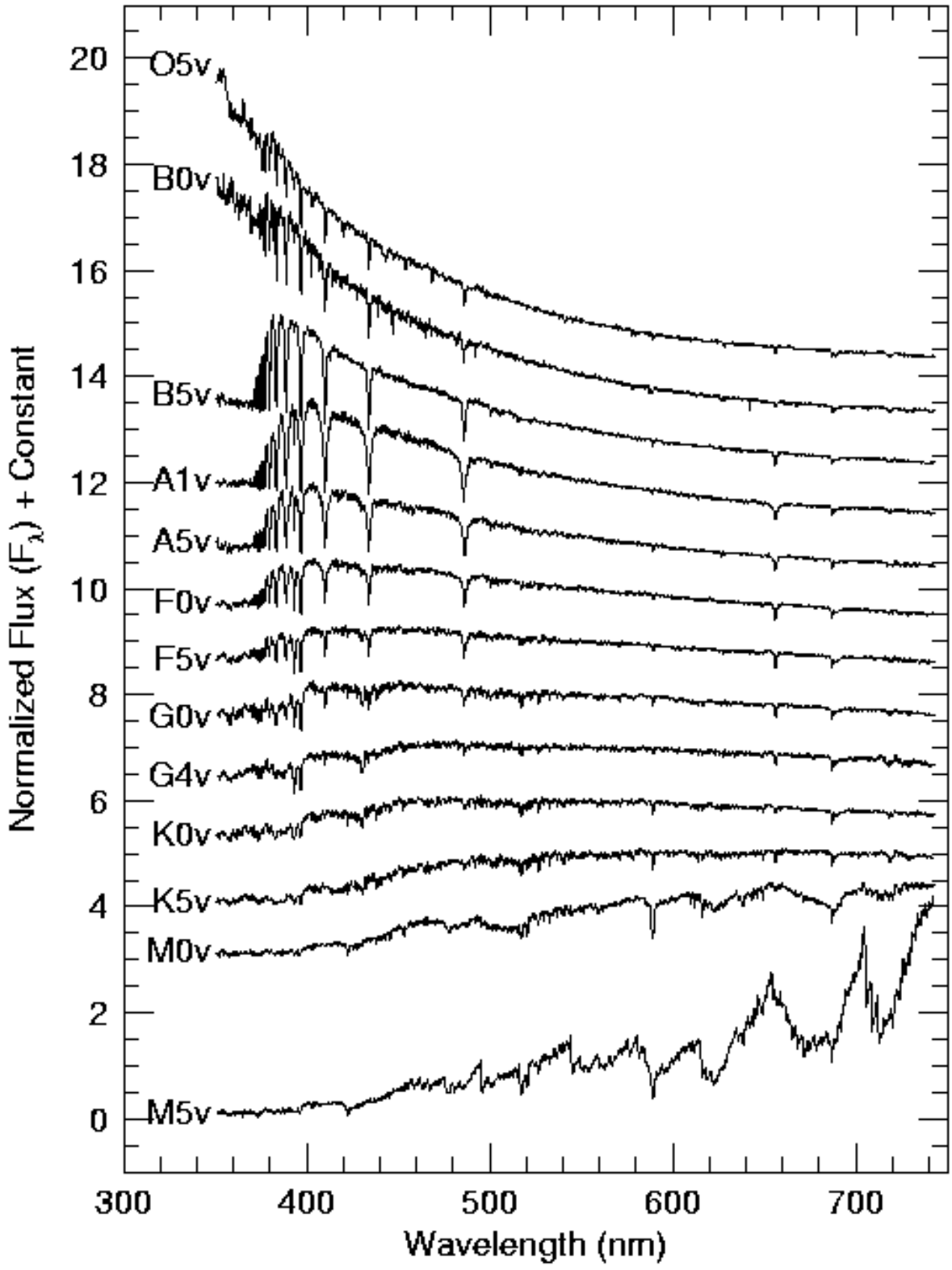

Fig. 15.— Low dispersion spectra of stars of various spectral types assembled into a figure. Earlier spectral classes (hotter stars) are at the top, the cooler stars with TiO bands are at the bottom. Data are from Jacoby, Hunter & Christian, 1984, ApJS, 56, 257.

A classification of stellar spectra according to luminosity for a given spectral type; it was introduced as part of the Morgan-Keenan classification. The luminosity class broadly indicates whether a star is a dwarf (that is, a main sequence star), a giant, or a supergiant, since luminosity is directly related to surface area. Luminosity class is expressed as a Roman numeral, from I to V, and appears after the spectral type; for example, Tau Ceti, with spectral type G8, is listed as a G8V object.

Luminosity class	Description
Ia-0	Hypergiant (extreme supergiant)
Ia	Bright supergiant
Iab	Normal supergiant
Ib	Subluminous supergiant
II	Bright giants
III	Normal giants
IV	Subgiant
V	Main-sequence (dwarf) star

Related category

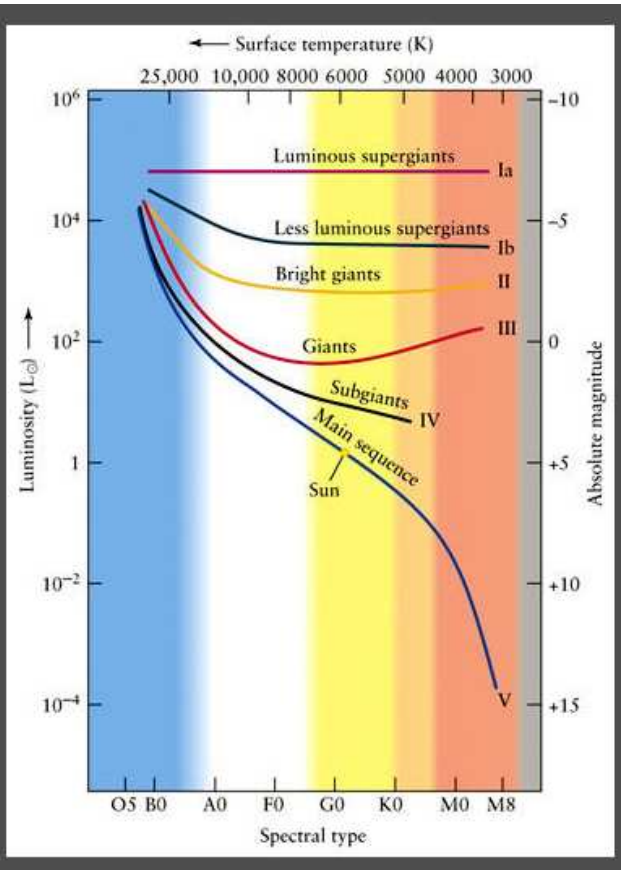

Fig. 16.— Stellar luminosity classes. Their spectra are affected by the difference in pressure in their atmospheres, higher pressure produces broader wings in strong lines.

Special classes of stars

Periodic Variables

Cepheids P 1 to 20 days, assymetric light curve, spectral class F with $M \sim 5M_{\odot}$ and age < 0.1Gyr

Miras Very long period red variables, P 8 - 1000 days, vary by up to a factor of 50, highly evolved

RR Lyrae P < 1 day, $M_V \sim 0$, low metallicity, low mass

W Virginis stars P $\sim 7 - 60$ days, old stars

High mass loss rate stars

Herbig-Haro stars Protostars with long jets

OH-IR Stars 1612 MHz OH line is seen in emission, high luminosity in the mid-IR

Wolf-Rayet Stars Very hot stars, losing mass very rapidly, spectra show broad emission lines of C or N, no hydrogen

Explosive Variables

Dwarf Novae short period binary, white dwarf + G, K or M main sequence star, ocassional eruptions by up to a factor of 100 in luminosity from instabilities in the accretion disk, varations in the mass transfer rate, etc.

Novae Luminosity up by a factor of 500 or more during eruption, close binary, mass containing accretes onto lower mass component and H eventually ignites, ejection velocity $v_{ej} \lesssim 3000$ km/sec.

Supernovae Violent explosion, $v_{ej} \sim 10,000$ km/sec.

Effective Temperature

L = emitting area × energy emitted = $4\pi R^2 \sigma T_{eff}^4$.

For the Sun, $T_{\rm eff}$= 5780 K, and $L = 3.8 \times 10^{33}$ ergs/sec.

The range for stars: $10^{-3} < L/L_\odot < 10^5$ (range of 10^8 !)

10^3 K $< T_{\rm eff} < 10^5$ K (range of only 100)

Surface Gravity

The local gravity at the surface of a star is the surface gravity, g, $g = GM/R^2$, $g_\odot = 2.7 \times 10^4$ cm/sec^2. Recall that g at the surface of the Earth is 980 cm/sec^2.

Spectral Energy Distributions of Stars

SEDs of stars are *almost* a black body, but not quite. SEDs for galaxies are the sum of many different stars, so further from a single T blackbody, and distinct from those of individual stars.

Planck function, flux emitted by a blackbody, $B_\nu = \frac{2h\nu^3}{c^2} e^{h\nu/kT}$ ergs/cm2/sec/Hz

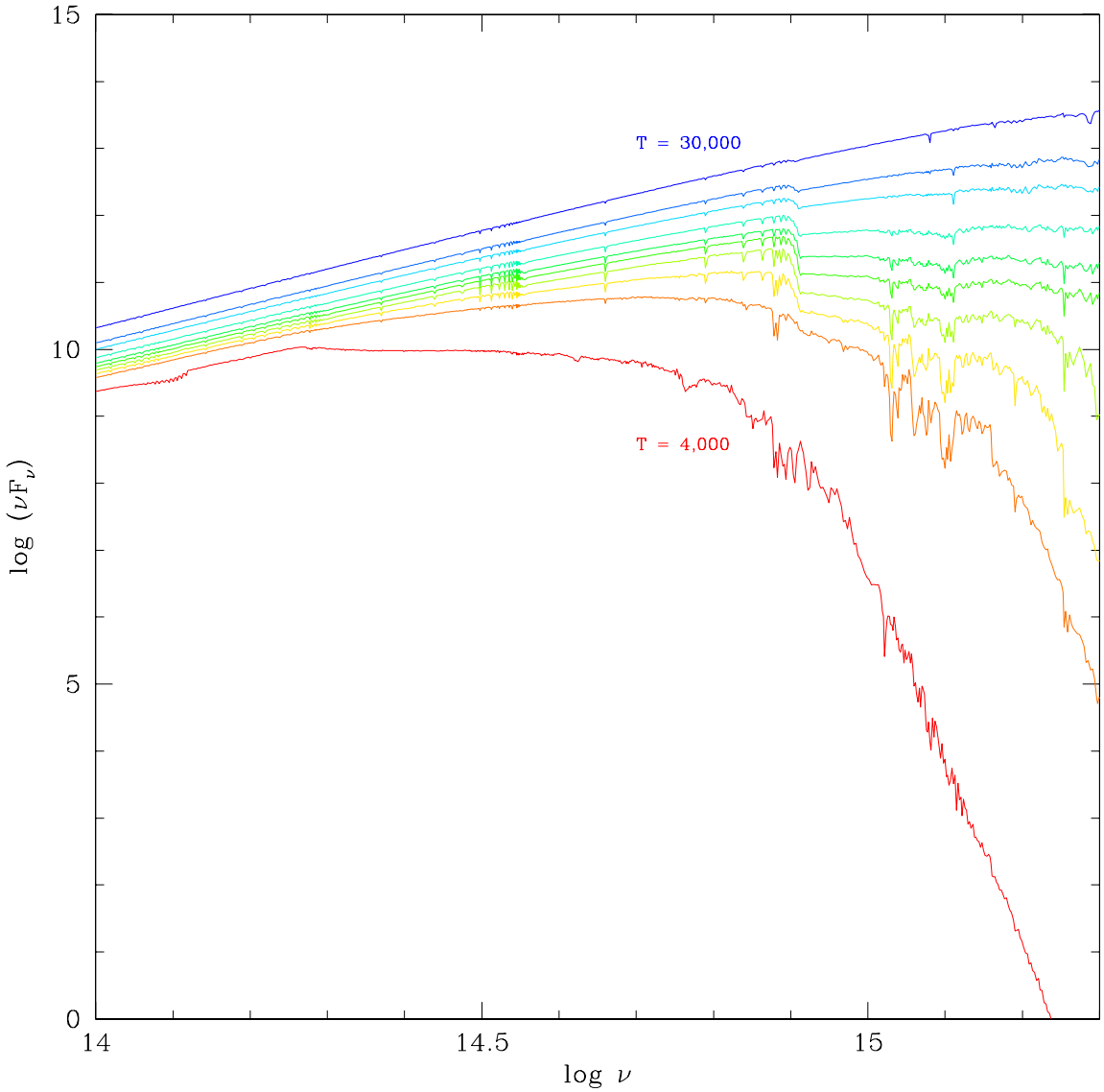

Fig. 19.— The spectral energy distribution of model stellar atmospheres of main sequence stars as a function of $T_{\rm eff}$. This figure is from R.L.Kurucz.

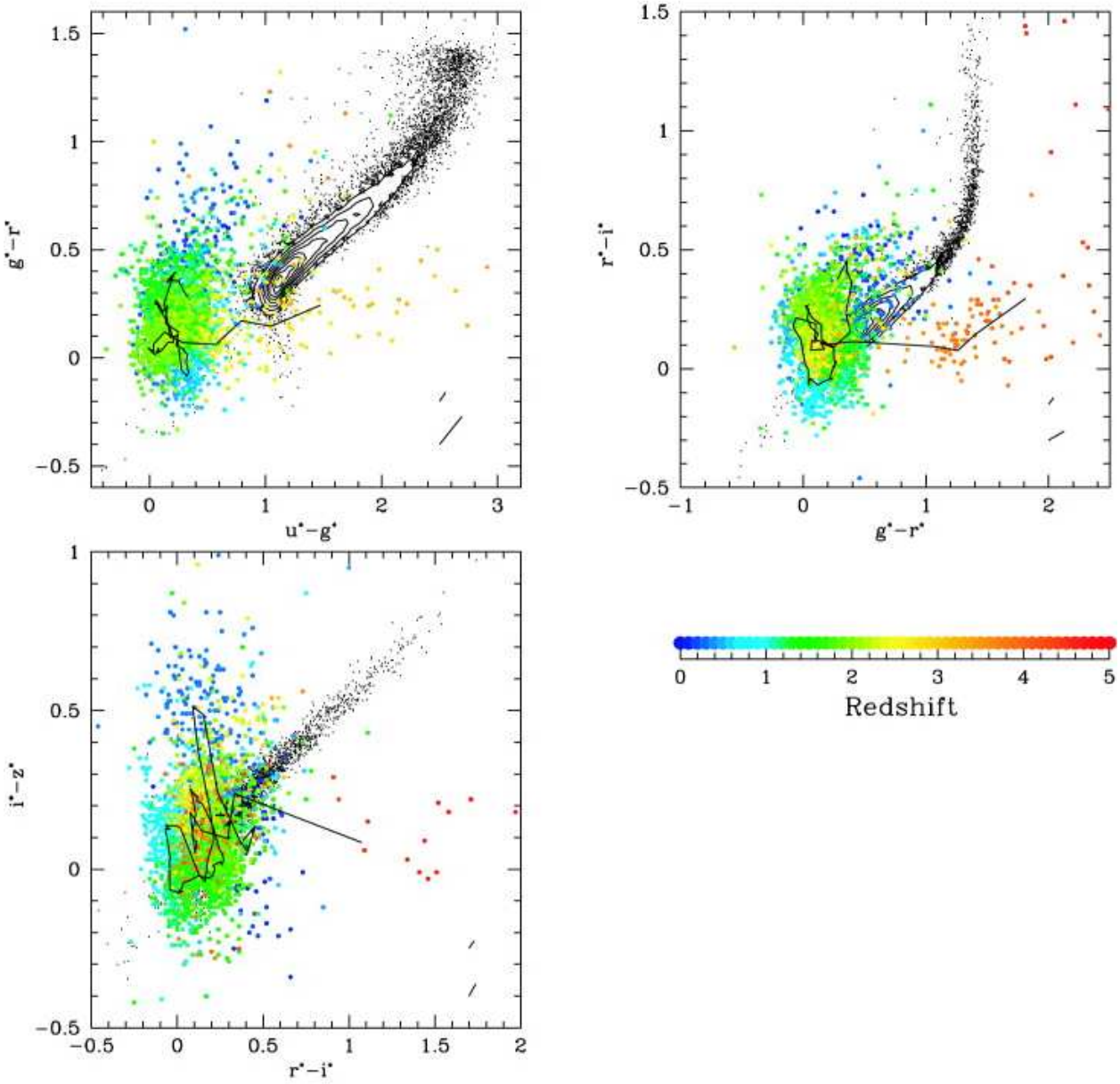

Fig. 20.— Color-color plots (3 different sets of filters) for stars from the SDSS (black points) and for QSOs (color encodes redshift as indicated in the legend). Note the concentration over a relatively range in color of the stellar population. This is figure 4 of Richards et al, Colors of 2625 QSOs from SDSS, AJ, 2001, 2308. (see also the 3D visualization of this in Fan et al, AJ, 117, 254)

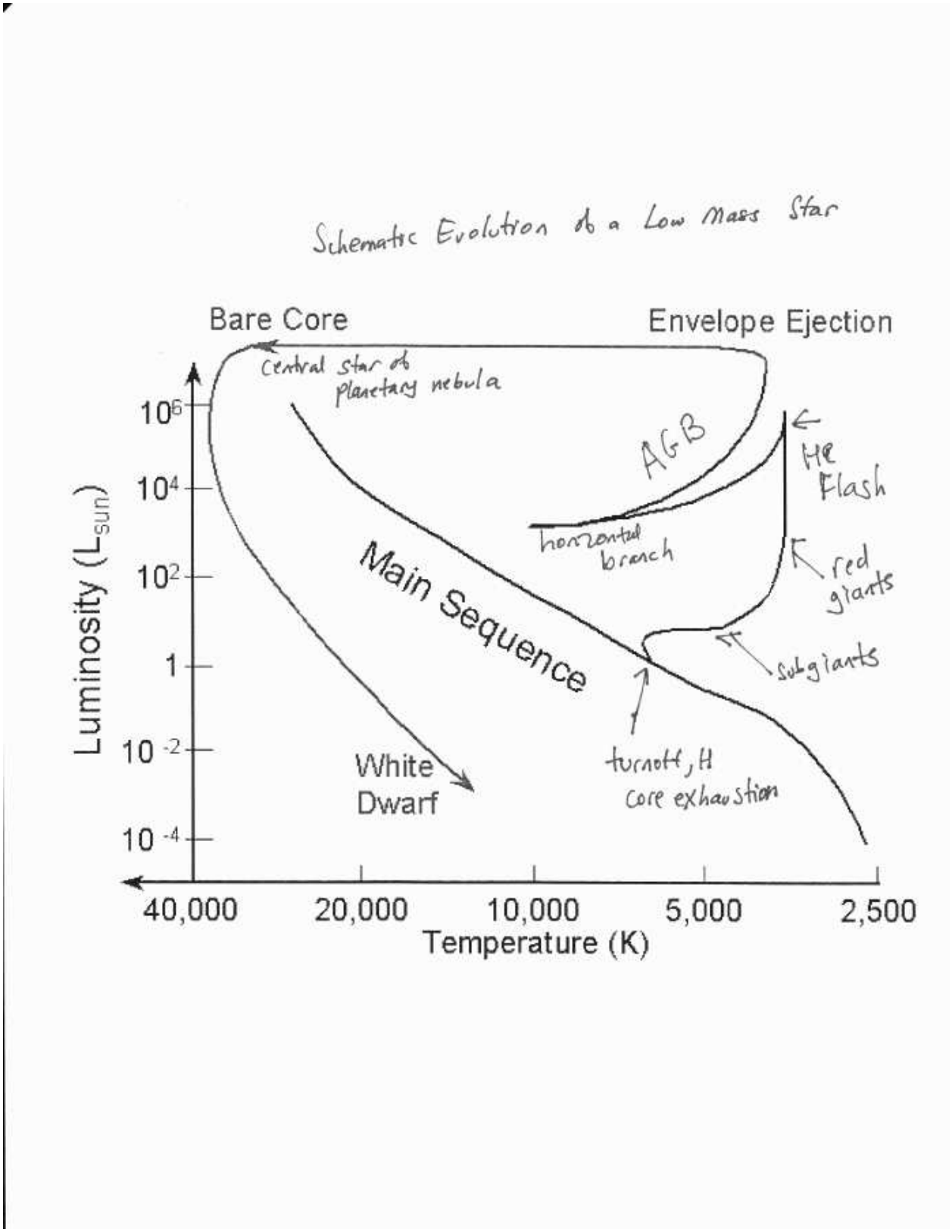

Fig. 21.— A schematic of stellar evolution for a star with a mass similar to that of the Sun.

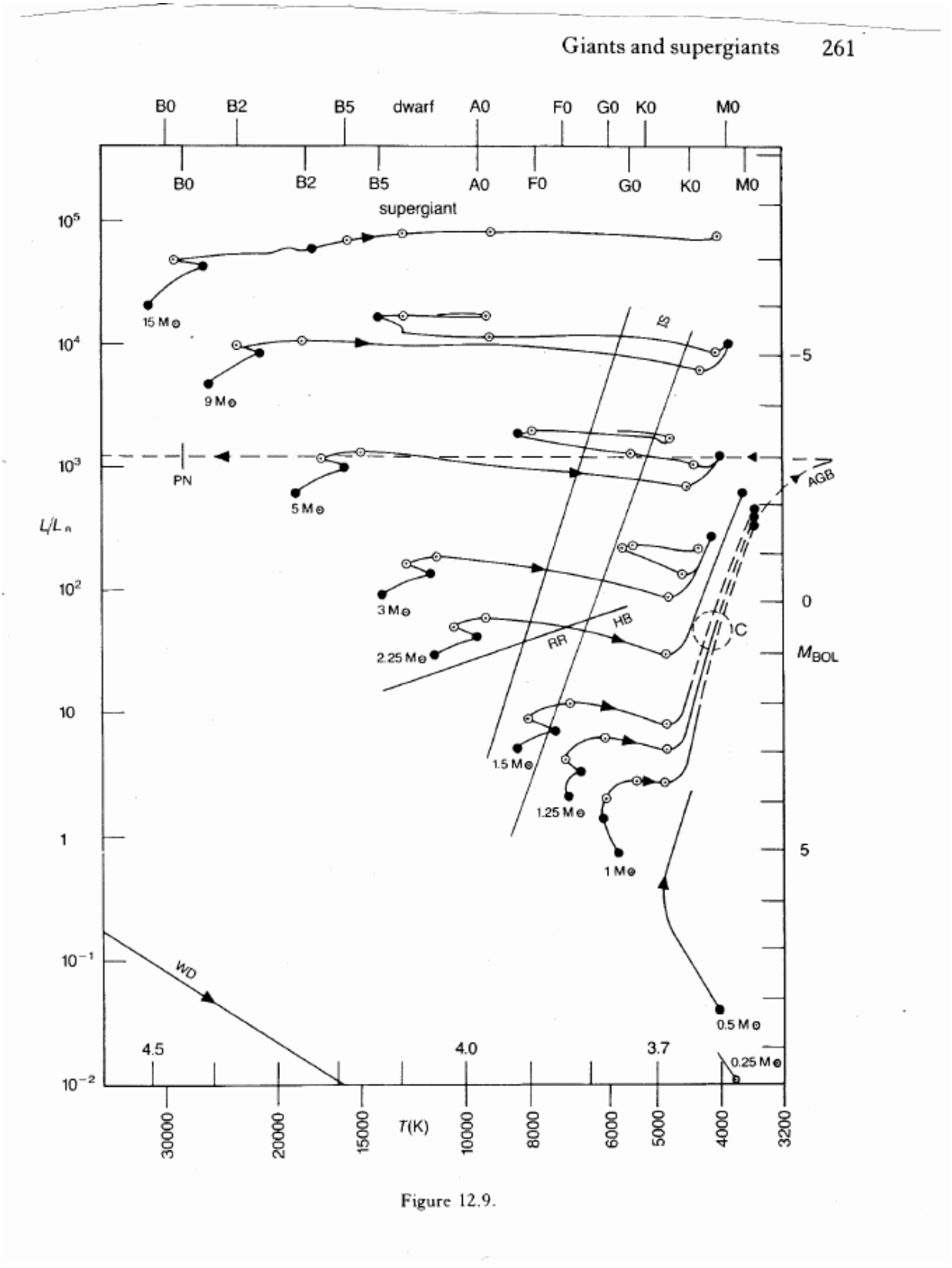

Figure 12.9.

Fig. 22.— Evolution off the main sequence for stars of a wide range of masses. These are stellar tracks from Icko Iben; see fig. 3 of Iben, ARAA, 1967, 5, 571, but the actual figure is

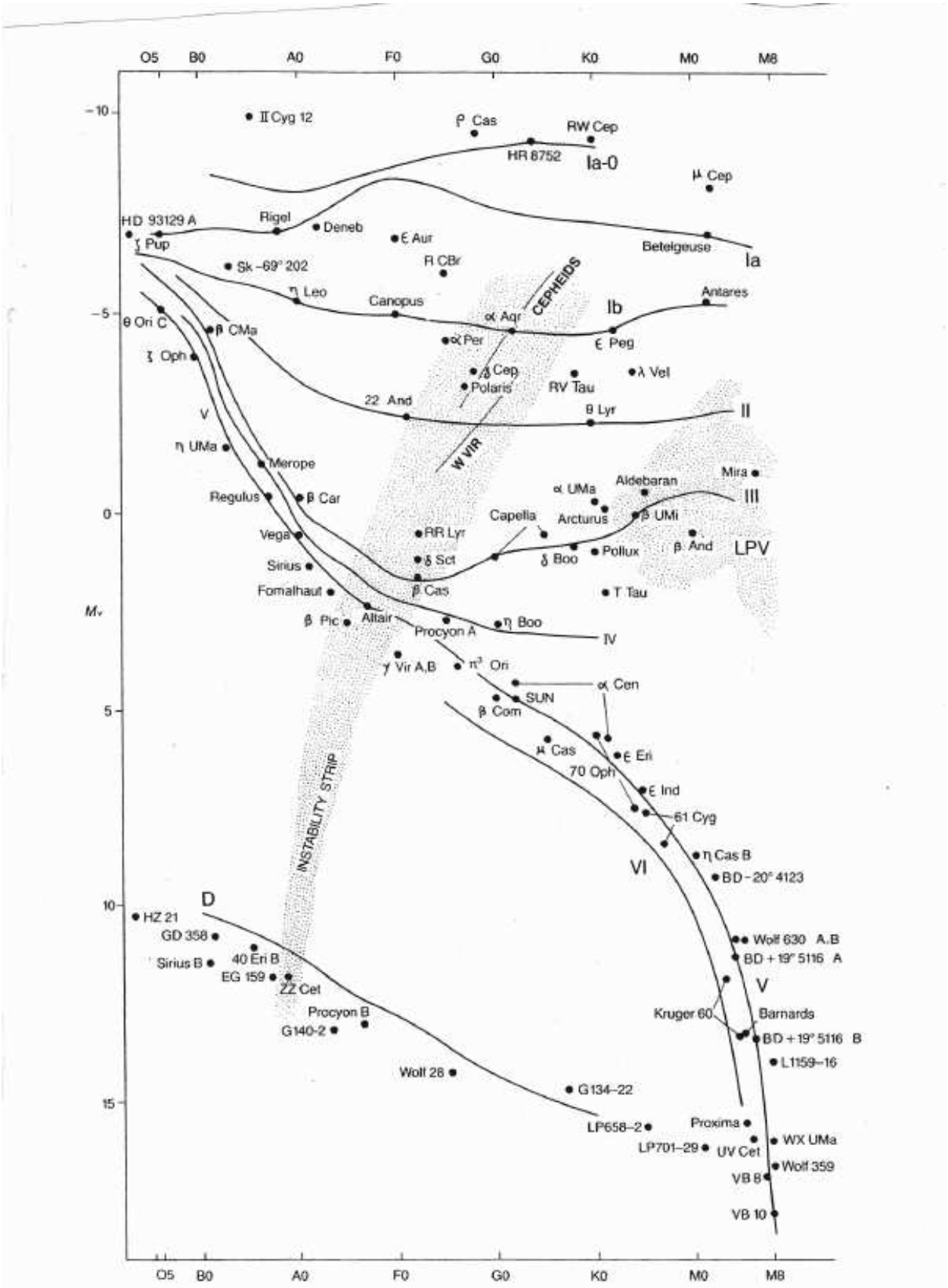

Figure 12.7. The completed HR diagram. Stellar data were taken from *The Bright Star Catalogue*, 4th rev. edn., by D. Hoffleit with the collaboration of C. Jaschek, Yale University Observatory, 1982, and from *Astrophysical Quantities*, 3rd edn., by R. H. Allen, Athlone Press, London, 1973. See Figure 3.8 for further

6. Star Clusters

Star clusters have special importance in studying stellar characteristics and evolution. They represent a group of stars formed at approximately the same time, same age, same chemical composition. They are very useful for testing model predictions.

Isochrones are calculated from tracks of stellar evolution for stars of a wide range in stellar mass. Isochrones are assembled by connecting the value of a parameter at a fixed time from tracks of various masses. Thus they predict A as a function of M for a fixed time. Since clusters of stars often contain stars of a fixed age and chemical composition the behavior of any parameter of interest for the sample of cluster members can be represented by an isochrone plot of the parameter A for $t =$ the age of the cluster.

In general, young clusters are not fully virialized and may not be bound against the Galactic tidal field or passages through the Galactic plane. Young clusters contain stars of a wide range in mass.

Old "globular clusters", found in the Galactic halo, are massive clusters which are dynamically evolved and have ages of $\sim$10 Gyr, so they probe the evolution of low mass stars, all older stars having evolved through stellar death.

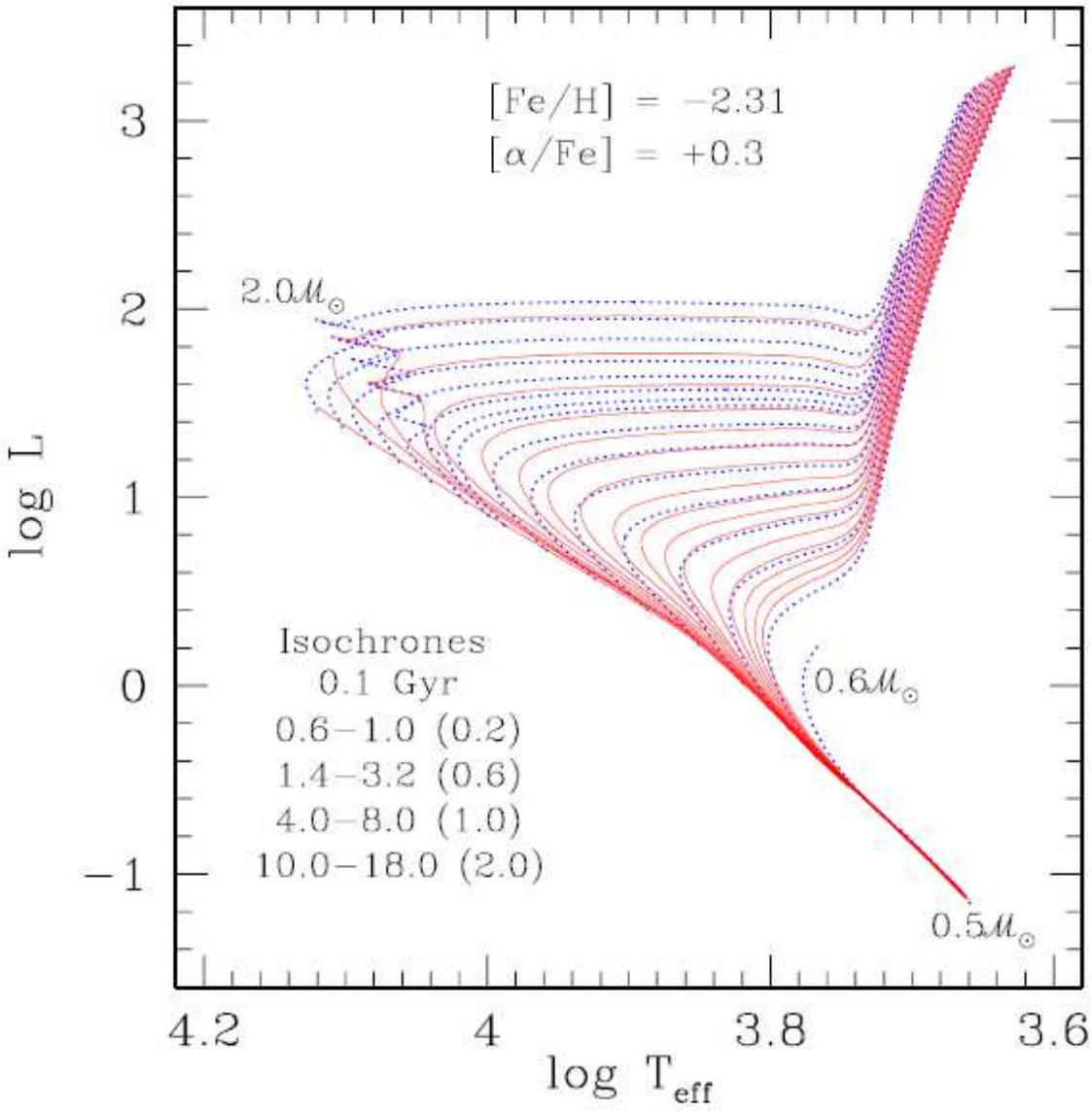

Fig. 9.— The complete grid of evolutionary tracks for the [Fe/H]= −2.31, [α/Fe] = +0.3 grid are plotted with the dotted blue lines. The tracks are spaced at 0.1$\mathcal{M}_\odot$ intervals with an additional track at 1.44$\mathcal{M}_\odot$, which is the transitional mass for the development of the blue hook. The isochrones, plotted as solid red lines, span the range of ages from 0.1 to 18.0 Gyr, as indicated.

Fig. 24.— Isochrones for stars of low metal content with ages from 0.1 to 18 Gyr. Note the overlap of all tracks for the lower main sequence where stars of low mass have not yet exhausted their H.

– 35 –

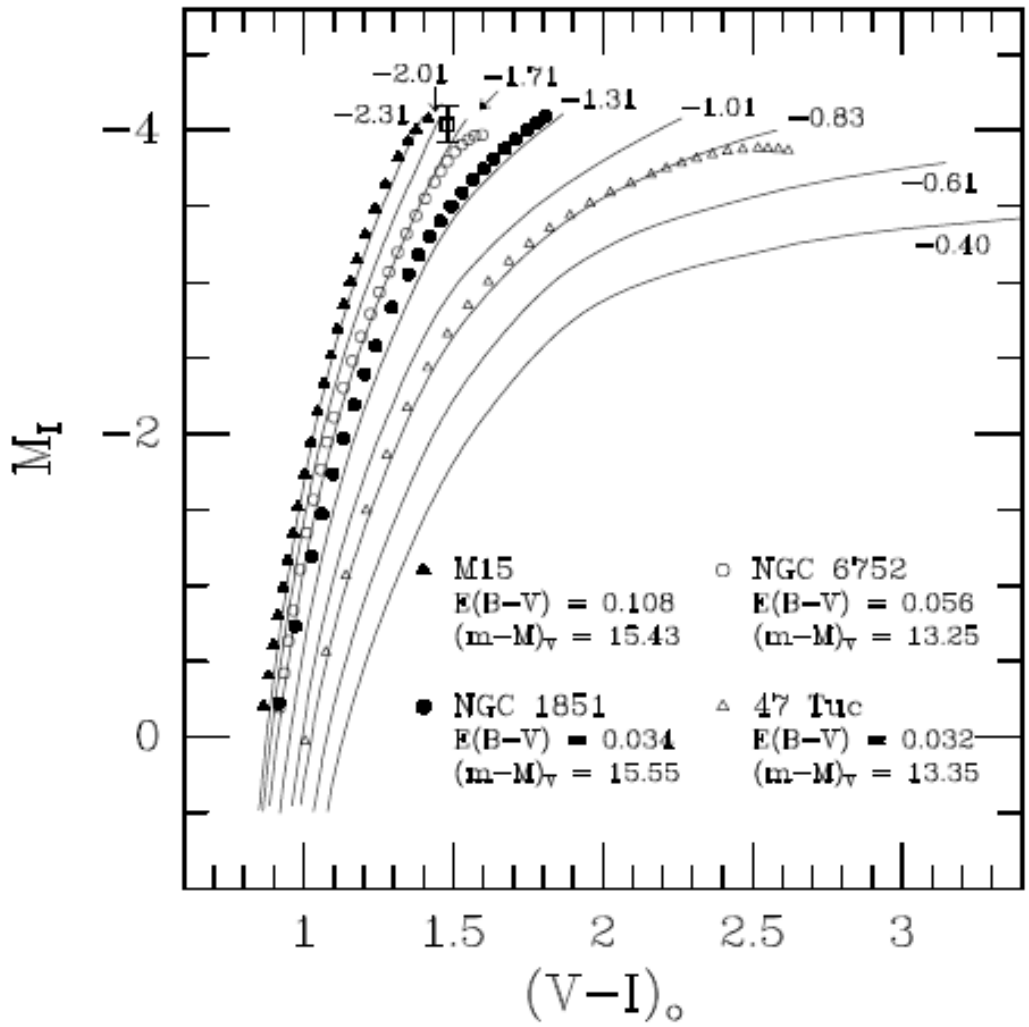

Fig. 13.— Overlay of the fiducial sequences derived by Da Costa & Armandroff (1990) for M15, NGC 6752, NGC 1851, and 47 Tucanae, on the assumption of the indicated reddenings and apparent distance moduli, onto the giant-branch segments of 13 Gyr isochrones for [Fe/H] values ranging from −2.31 to −0.40, assuming [α/Fe] = 0.3 in each case. Note that, as shown by VandenBerg (2000), turnoff ages close to 13 Gyr are consistent with the adopted $(m - M)_V$ values only for M 15 and NGC 6752: somewhat younger ages (≈ 11.5 Gyr) are obtained for NGC 1851 and 47 Tuc. The large open square, with error bars, gives the absolute I magnitude of the RGB tip stars in ω Centauri determined by Bellazzini et al. (2001); see the text.

Fig. 25.— Isochrones for stars of a range of metal content with a fixed age of 13 Gyr. Only the region of the red giant branch is shown. Fiducial lines for 4 well studied Galactic globular clusters are shown. Overlapping theory and data requires specifying the distance and the interstellar reddening of each cluster.

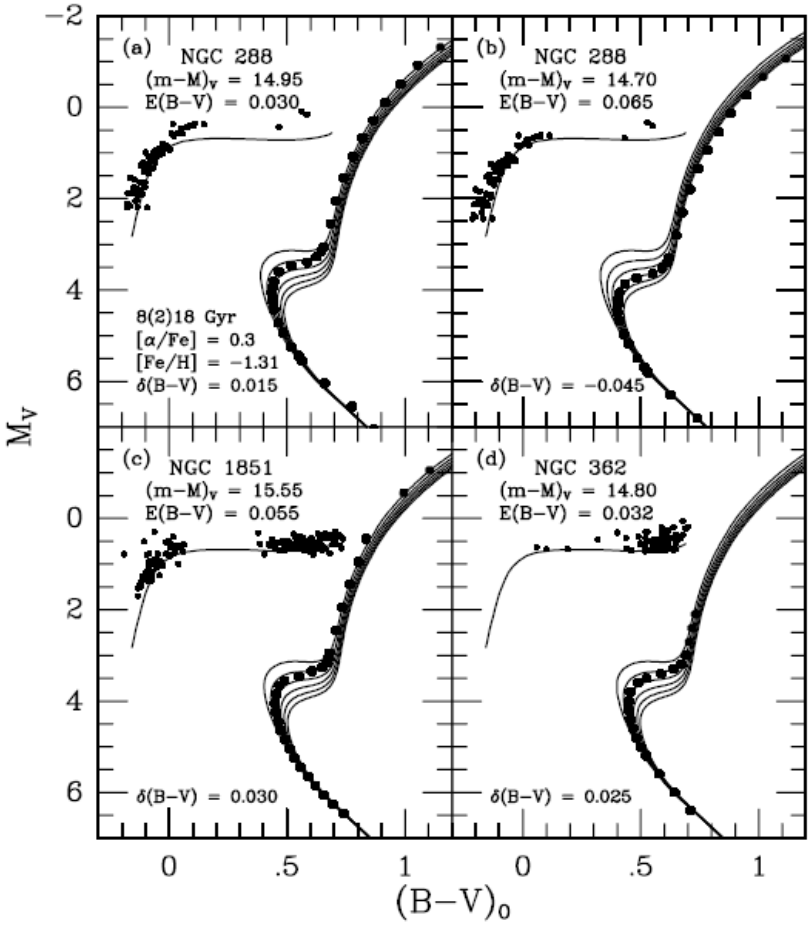

FIG. 28.—Panels (*a*) and (*b*) illustrate two of many possible fits of our ZAHB and isochrones for the indicated parameters to the NGC 288 CMD. The fiducial for the main sequence and giant stars is as defined in Fig. 23: the HB photometry is from Bergbusch (1993), but corrected by +0.01 mag in $B-V$ and −0.0635 mag in V to place those data on the system of Bolte (1992) photometry. Panels (*c*) and (*d*) show how well the same models match the NGC 1851 (Walker 1992b) and NGC 362 (VBS, Harris 1982) CMDs, respectively. The adopted reddening for the latter is from the SFD maps, while that for the former is based on the fit of the ZAHB to the blue HB stars (see the text for some discussion of this point).

Fig. 26.— Isochrones for stars of a range of metal content with a fixed age (13 Gyr ?). Fiducial lines for 4 well studied Galactic globular clusters are shown including the lower main sequence and the RGB. Individual horizontal branch stars are shown as well.

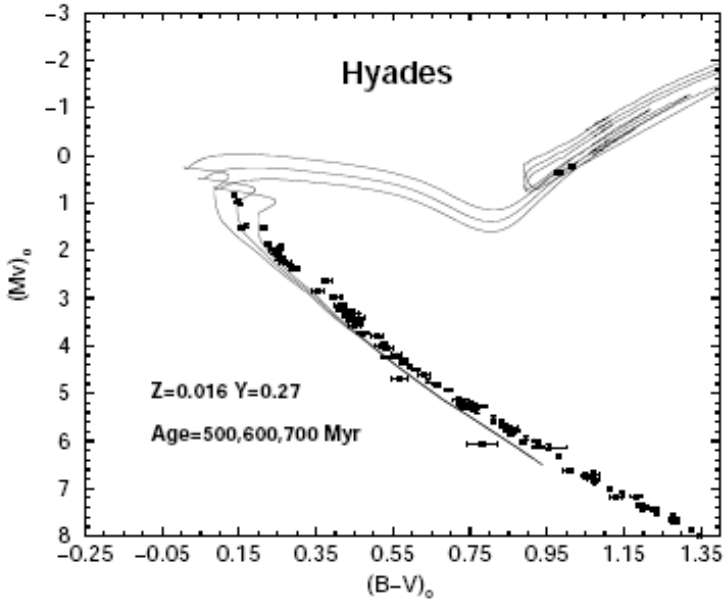

FIG. 3. The CMD for the Hyades, using the parallax values from Madsen et al. (2002). Visual, spectroscopical and suspected binaries are excluded, see also Madsen et al. (2000). Error bars indicate observational errors as given by Madsen et al. (2002) for the parallax and by the Hipparcos catalog (at the node http://astro.estec.esa.nl/Hipparcos/HIPcataloguesearch.html) for the colors. Observational data are compared with present theoretical isochrones for Z=0.016 Y=0.27 α=1.9. Color transformations and bolometric corrections from Castelli (1999).

Fig. 27.— Match of observations and theoretical isochrones for stars in the nearby Hyades cluster, believed to have an age of about 400 Myr. Note the presence of stars significantly more luminous (i.e. massive) than the Sun still on the main sequence.

7. The Endpoint of Stellar Evolution

Eventually nuclear fuels are completely consumed, at least in the hot central regions of the star. At that time, low mass stars more or less cease nuclear burning, and gradually fade in a quiescent fashion, becoming white dwarfs. These stars have central regions made mostly of He or of the CNO elements, with at most a thin outer layer of H.

The manner of "stellar death", for single non-rotating stars, depends on the initial mass of the star and on the amount of mass lost during its evolution. There will be extensive mass loss during the AGB, supergiant, and/or planetary nebula phases. Higher mass stars explode, becoming supernovae of various types. The remnant may be a neutron star (a pulsar perhaps), a black hole, or in the case of certain violent explosions, no remnant left at all. The nature of the remnant depends on the stellar mass (and to a lesser extent, its metallicity).

The material ejected from the supernova into the insterstellar medium contains heavily processed material, both from nuclear burning prior to the SN, and nuclear burning during the SN itself, which enriches the ISM in metals. The heavy metal content of the ISM rises with time due to mass loss from evolved stars (AGB, PN nuclei, etc) as well as from SN.

Type Ia SN, which do not show any lines of H in their spectra, are believed to arise from interactions in evolved binary stellar systems. These involve lower mass stars in general. Since the timescales for stars increase rapidly as the stellar mass decreases, there will be a delay in the appearance of Type Ia SN compared to the Type II SN occuring as the endpoint of stellar evolution for single massive stars. Since these contribute different sets of elements to the ISM, this delay can in principle be observed by studying the chemical evolution of the ISM with time, measured through unevolved stars of different ages.

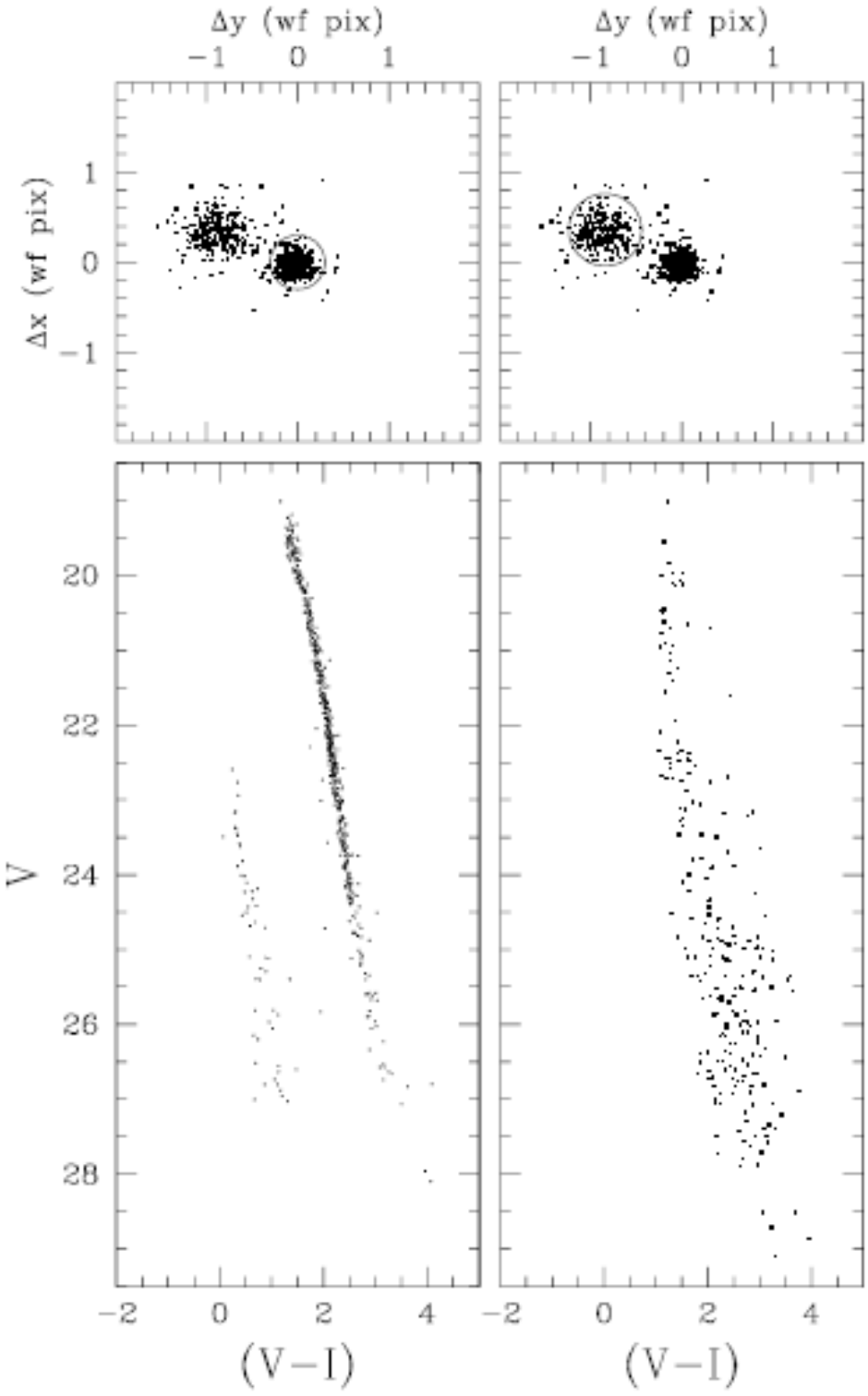

JPG

Fig. 29.— The lower main sequence and the sequence of low luminosity small radius white dwarfs in the globular cluster M4. The white dwarf sequence basically represent a cooling locus.

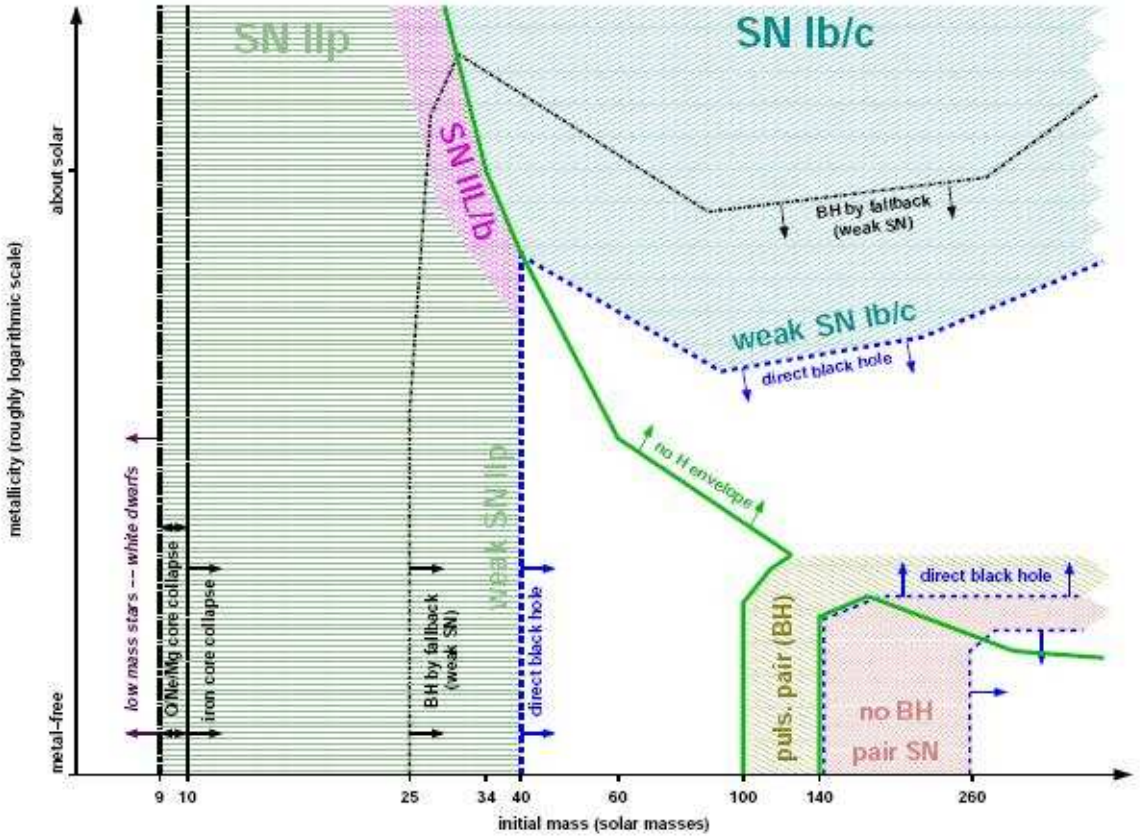

Fig. 2.— Supernovae types of non-rotating massive single stars as a function of initial metallicity and initial mass. The lines have the same meaning as in Fig. 1. *Green horizontal hatching* indicates the domain where Type IIp supernovae occur. At the high-mass end of the regime they may be weak and observationally faint due to fallback of ^{56}Ni. These weak SN Type IIp should preferentially occur at low metallicity. At the upper right edge of the SN Type II regime, close to the *green line* of loss of the hydrogen envelope, Type IIL/b supernovae that have a hydrogen envelope of $\lesssim 2\,M_\odot$ are made (*purple cross hatching*). In the upper right quarter of the figure, above both the lines of hydrogen envelope loss and direct black hole formation, Type Ib/c supernovae occur; in the lower part of their regime (middle of the right half of the figure) they may be weak and observationally faint due to fallback of ^{56}Ni, similar to the weak Type IIp SNe. In the direct black hole regime no "normal" (non-jet powered) supernovae occur since no SN shock is launched. An exception are pulsational pair-instability supernovae (lower right corner; *brown diagonal hatching*) that launch their ejection before the core collapses. Below and to the right of this we find the (non-pulsational) pair-instability supernovae (*red cross hatching*), making no remnant, and finally another domain where black hole are formed promptly at the lowest metallicities and highest masses (*while*) where nor SNe are made. White dwarfs also do not make supernovae (*white strip* at the very left).

Fig. 30.— The mode of stellar death as a function of initial stellar mass. Low mass stars become white dwarfs, while stars with $M \gtrsim 8_\odot$ become SN of various types.

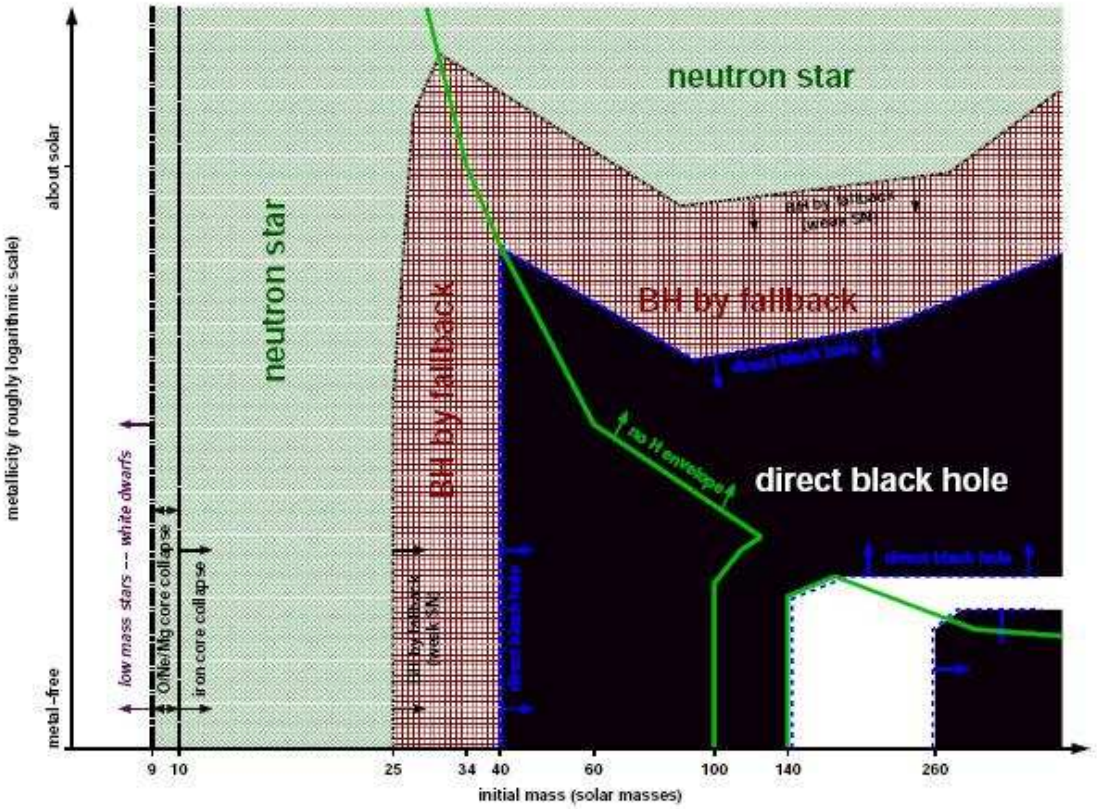

Fig. 1.— Remnants of massive single stars as a function of initial metallicity (*y-axis*; qualitatively) and initial mass (*x-axis*). The *thick green line* separates the regimes where the stars keep their hydrogen envelope (left and lower right) from those where the hydrogen envelope is lost (upper right and small strip at the bottom between 100 and 140 $M_{\odot}$). The *dashed blue line* indicates the border of the regime of direct black hole formation (*black*). This domain is interrupted by a strip of pair-instability supernovae that leave no remnant (*white*). Outside the direct black hole regime, at lower mass and higher metallicity, follows the regime of BH formation by fallback (*red cross hatching* and bordered by a *black dash-dotted line*). Outside of this, *green cross hatching* indicates the formation of neutron stars. The lowest-mass neutron stars may be made by O/Ne/Mg core collapse instead of iron core collapse (*vertical dash-dotted lines* at the left). At even lower mass, the cores do not collapse and only white dwarfs are made (*white strip* at the very left).

Fig. 31.— The remnant at the end stage of the evolution of a star is shown as a function of mass and metal content. Possibilities include white dwarfs, neutron stars, black holes, no remnent left at all, etc.

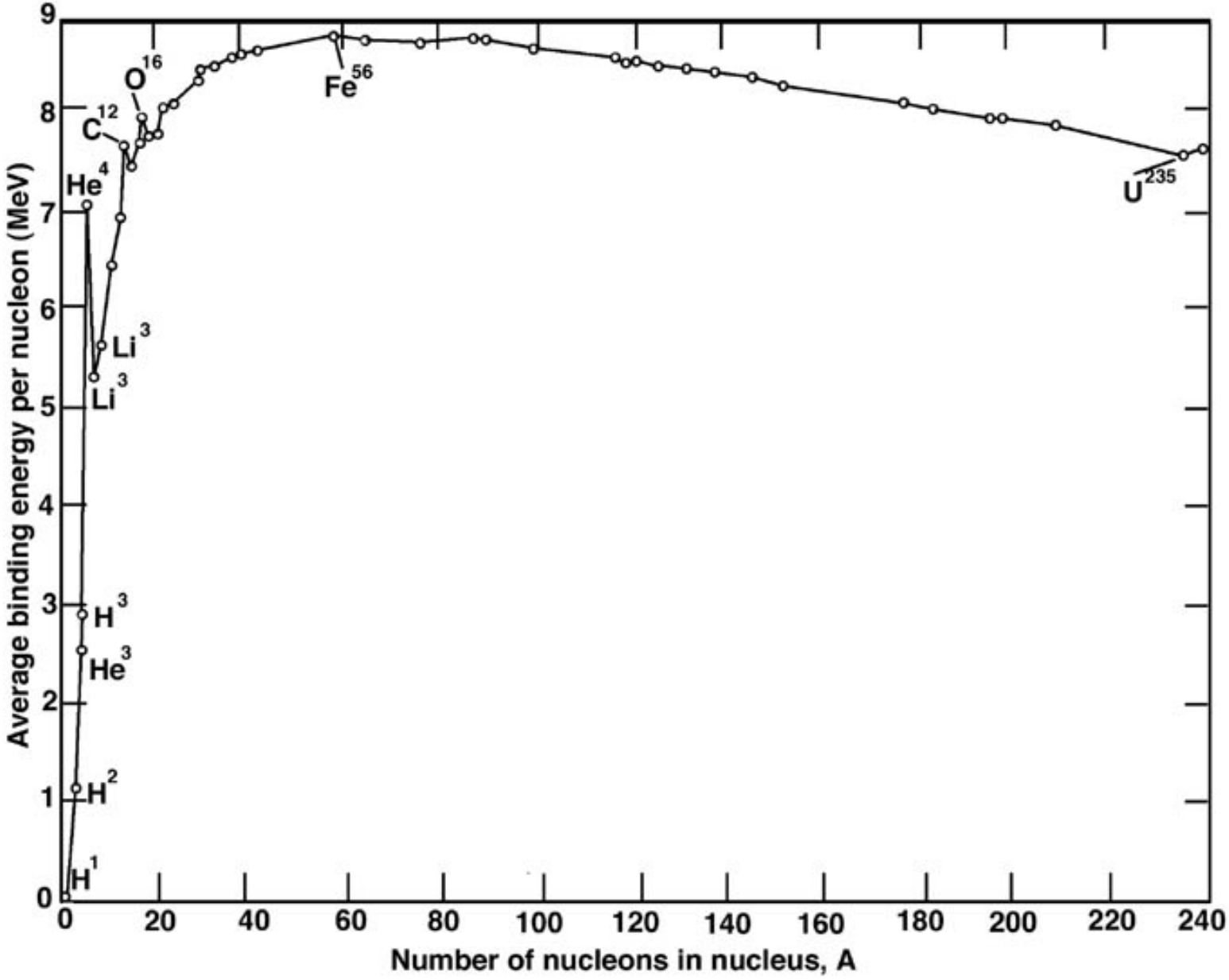
Average binding energy per nucleon (MeV)
Number of nucleons in nucleus, A
0
1
2
3
4
5
6
7
8
9
0
20
40
60
80
100
120
140
160
180
200
220
240
H1
H2
H3
He3
He4
Li3
Li3
C12
O16
Fe56
U235

Rank in ϵ_i	Element	$\log_{10}\epsilon_i$	Mass fraction X_i	Rank in X_i
1	O	$\sim$8.69	5.78×10^{-3}	1
2	C	$\sim$8.43	2.38×10^{-3}	2
3	Ne	$\sim$7.93	6.28×10^{-4}	7
4	N	$\sim$7.83	6.99×10^{-4}	5
5	Mg	$\sim$7.6	7.05×10^{-4}	4
6	Si	$\sim$7.5	6.69×10^{-4}	6
7	Fe	$\sim$7.5	1.31×10^{-3}	3
8	S	$\sim$7.12	3.11×10^{-4}	8

Top-abundant metals in the solar composition.
Following Asplund et al. 2009, ARAA, 47, 481

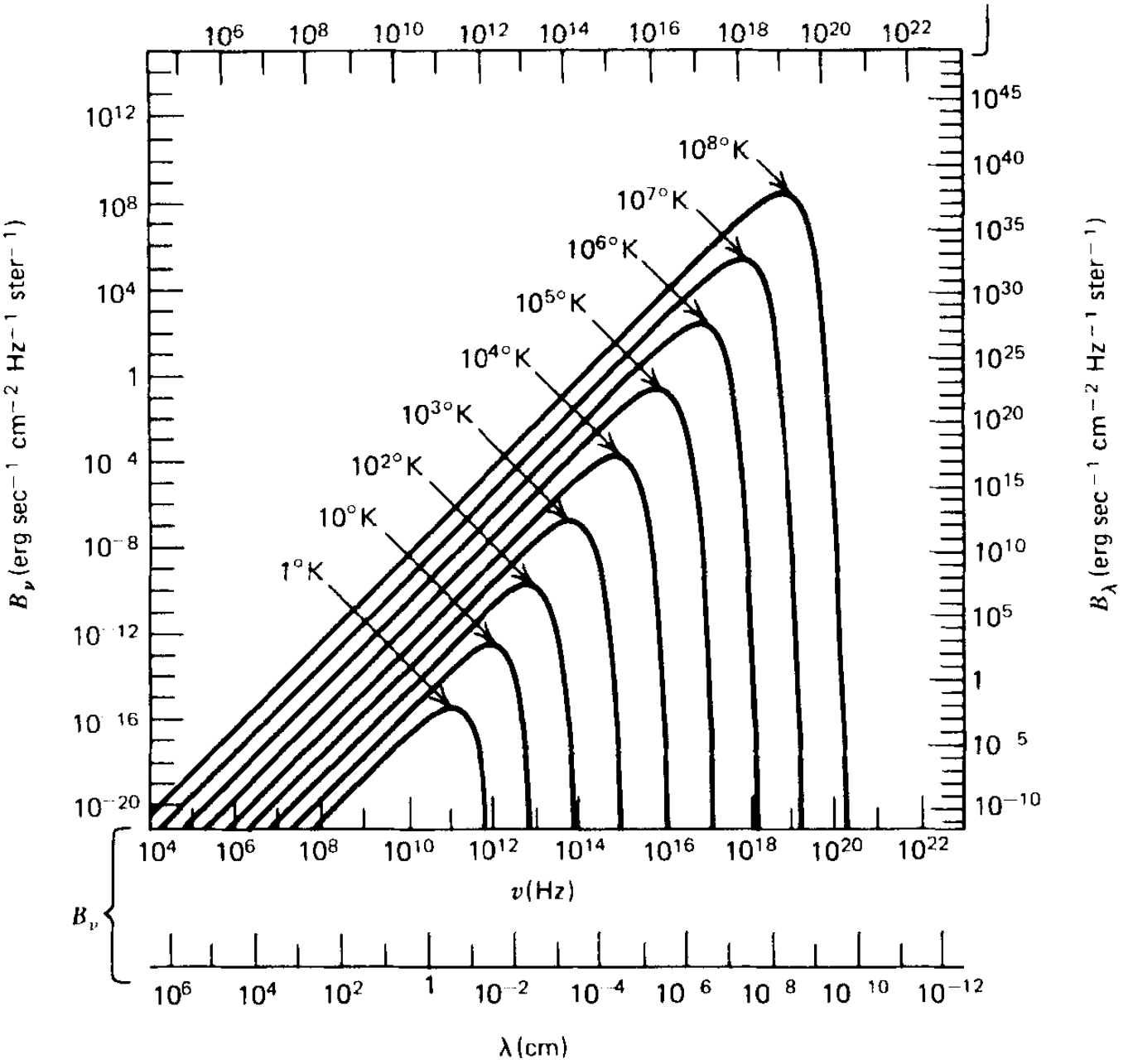

Figure 1.11 Spectrum of blackbody radiation at various temperatures (taken from Kraus, J. D. 1966, Radio Astronomy, McGraw-Hill Book Company)

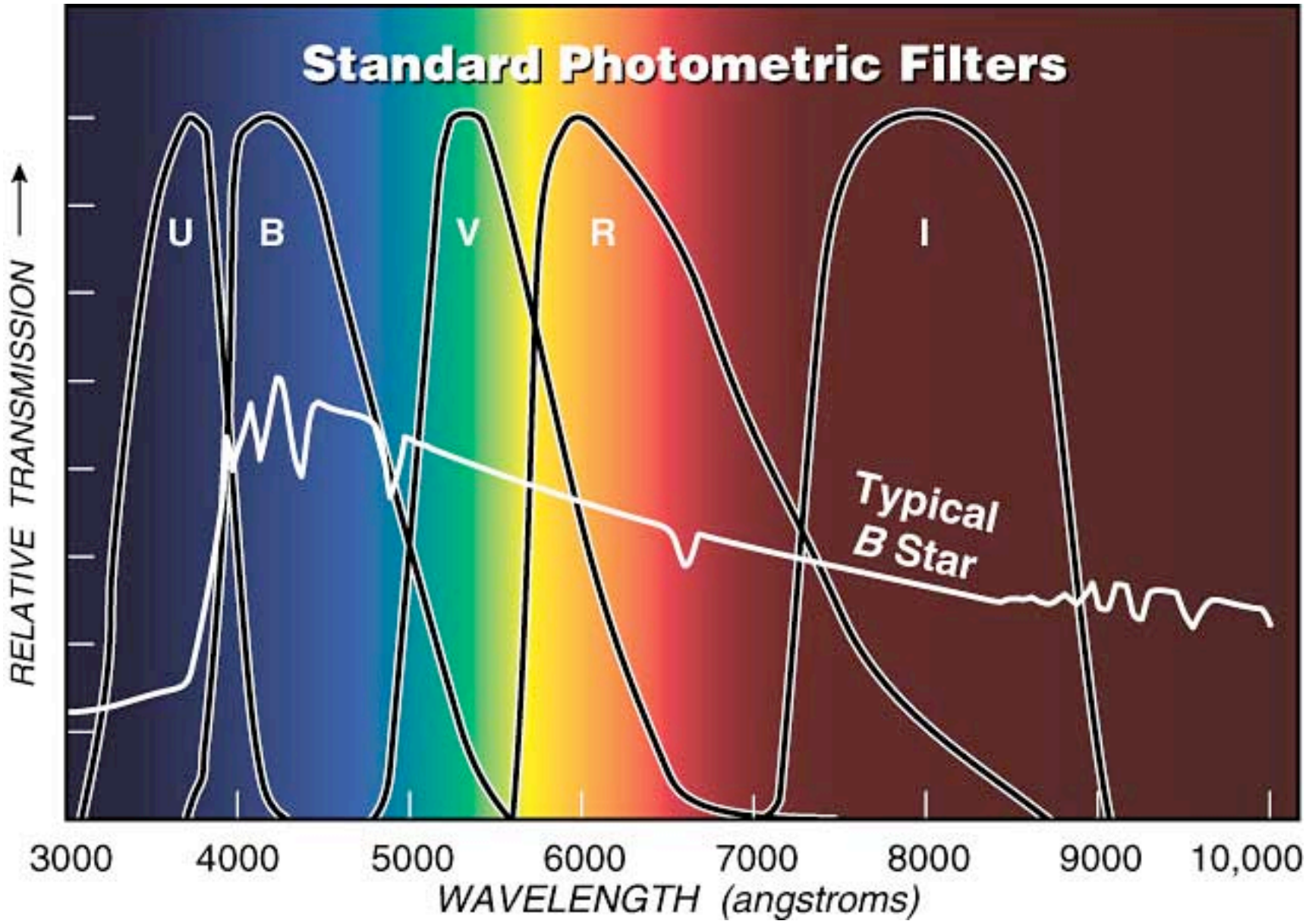

(Sky & Telescope)

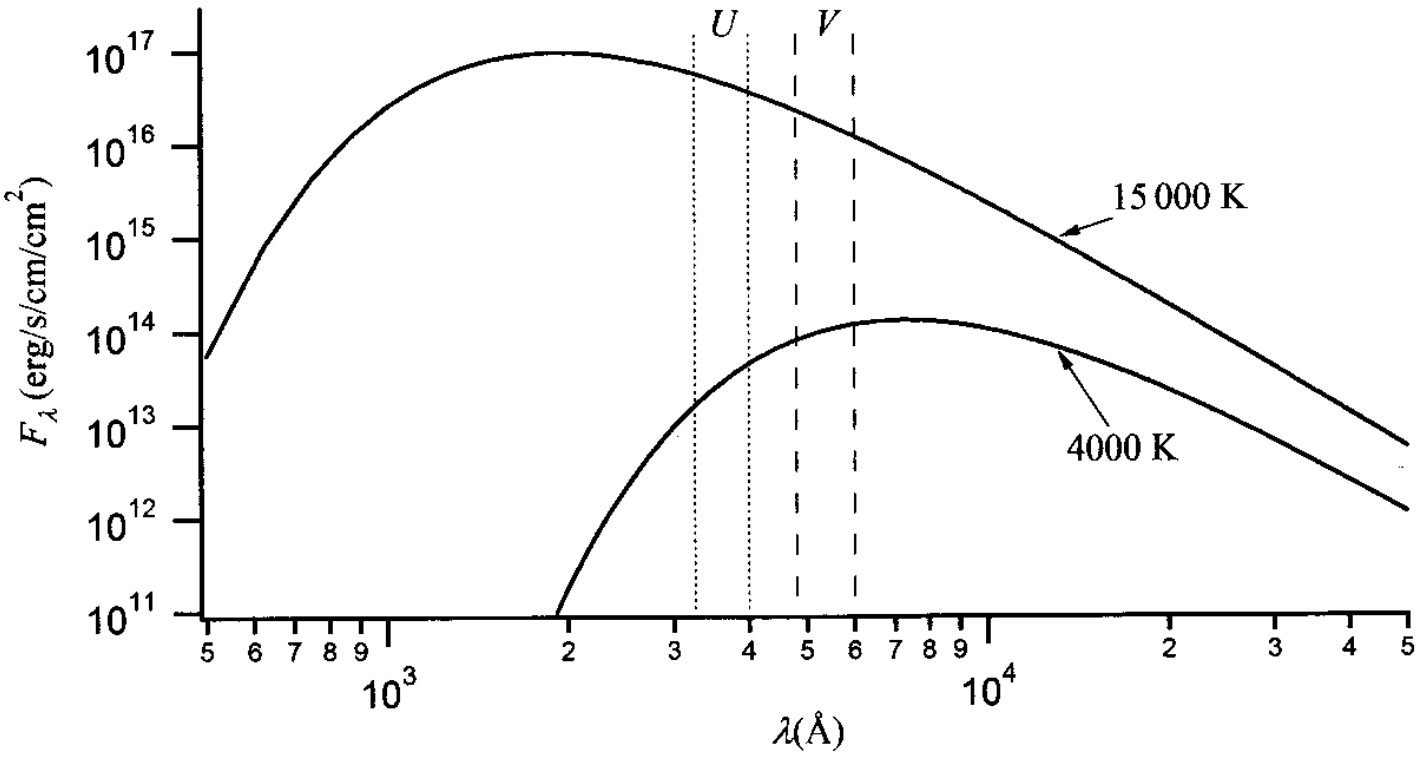

Figure 1.4 Monochromatic flux (F_λ) as a function of wavelength for two stars with T_{eff} = 4000 and 15 000 K approximated by blackbody radiation. The approximate positions of two photometric filters (U and V) are also shown.

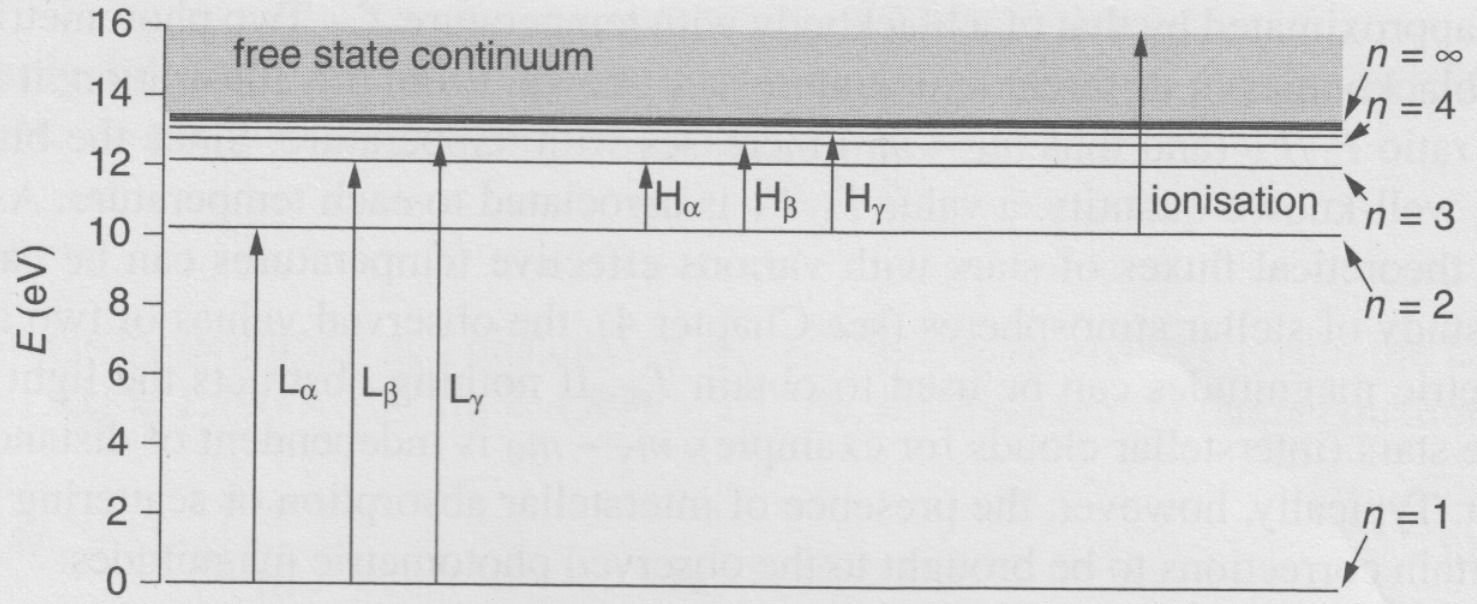

Figure 1.5 Energy levels of hydrogen in eV. Various bound-bound transitions are also shown, as well as a bound–free transition from level $n = 2$ (see Section 1.6 for more details).

LeBlanc – An Introduction to Stellar Astrophysics

Balmer emission spectrum (Source: Wikipedia)

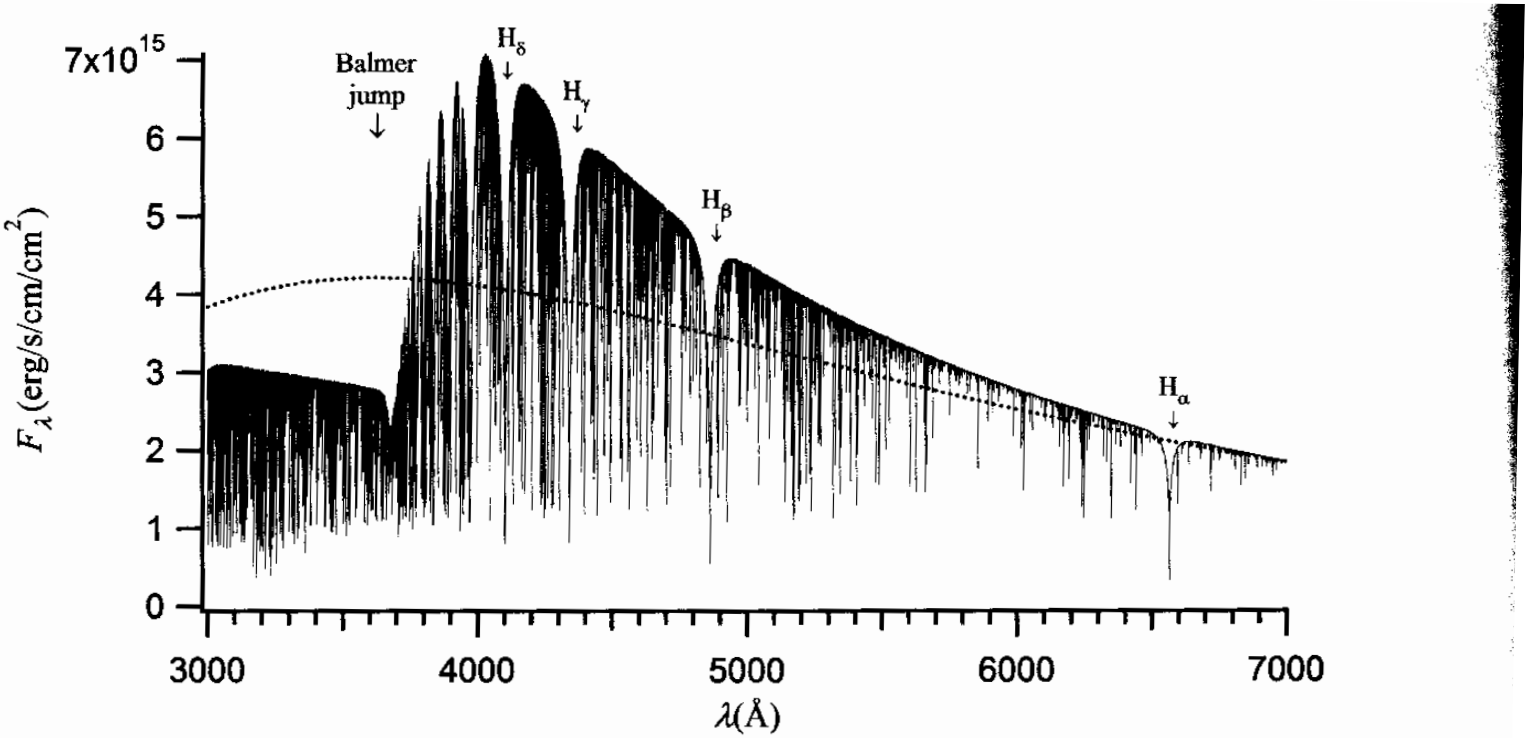

Figure 1.8 Theoretical monochromatic flux emerging form an A type star with $T_{\text{eff}} = 8000\,\text{K}$. The first four Balmer absorption lines, as well as the Balmer jump, are identified in this figure. Thousands of other absorption atomic lines can also be seen. This theoretical flux was obtained with the Phoenix stellar atmosphere code (Hauschildt, P.H., Allard, F. and Baron, E., *The Astrophysical Journal*, **512**, 377 (1999)) while using the elemental abundances found in the Sun. The flux at the surface of a blackbody with $T = 8000\,\text{K}$ (dotted curve) is also shown.

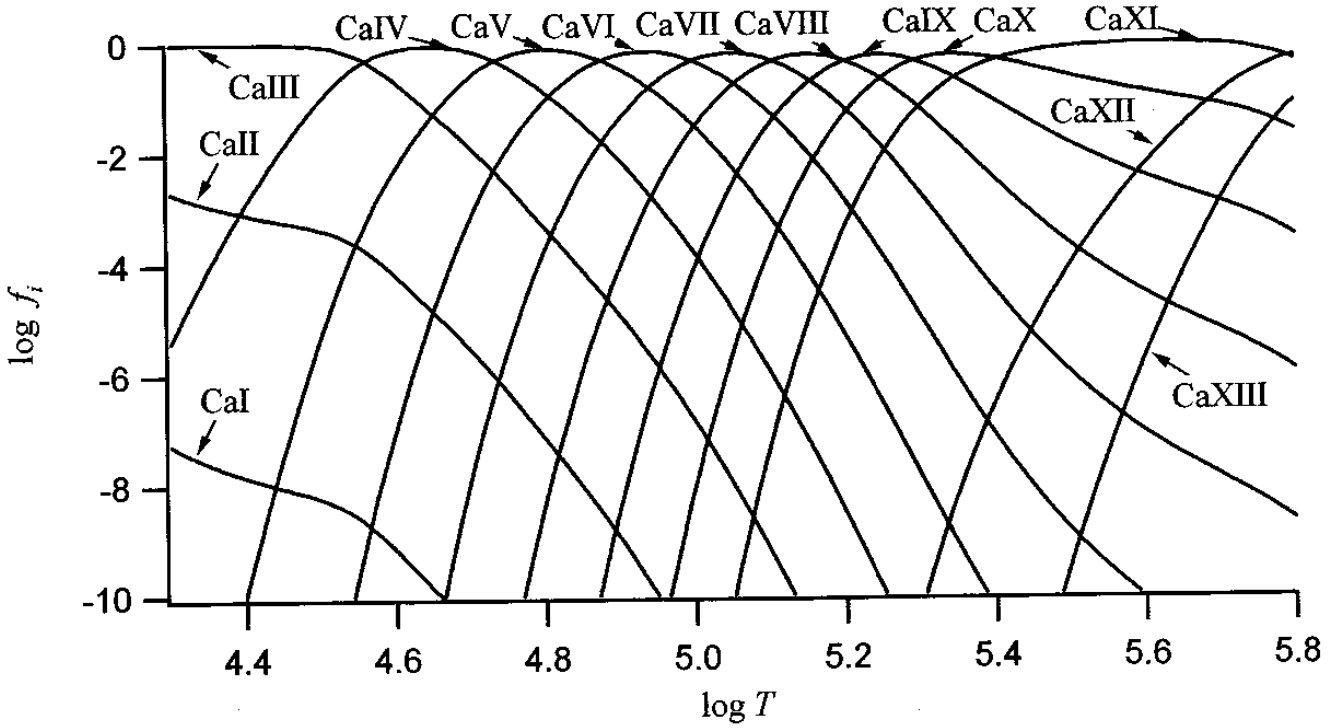

Figure 1.7 Ionisation fractions (f_i) of Ca ions as a function of temperature (or depth) in the interior of a star with $T_{\rm eff}$ = 7600 K. The surface of the star is found at the left side of the horizontal axis.

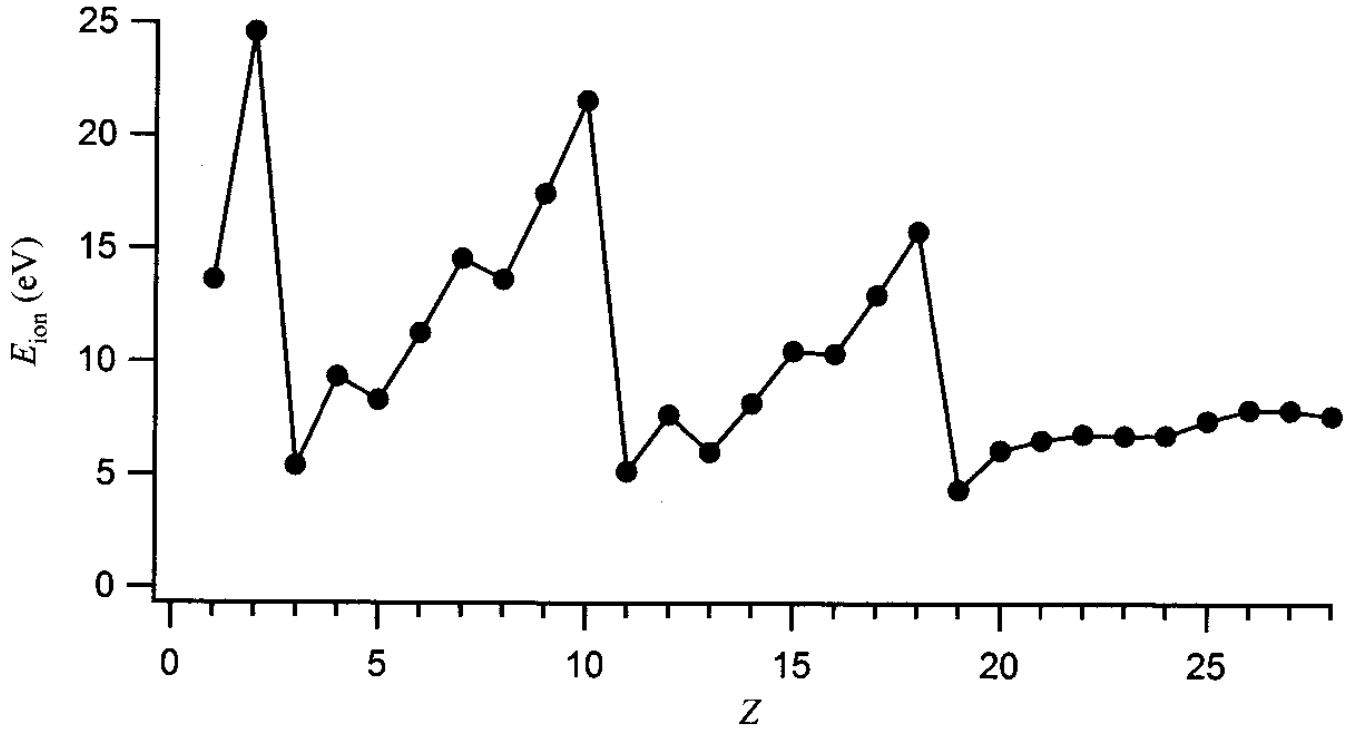

Figure 1.6 Ionisation energy (from the fundamental atomic energy state) as a function of atomic number for neutral atoms.

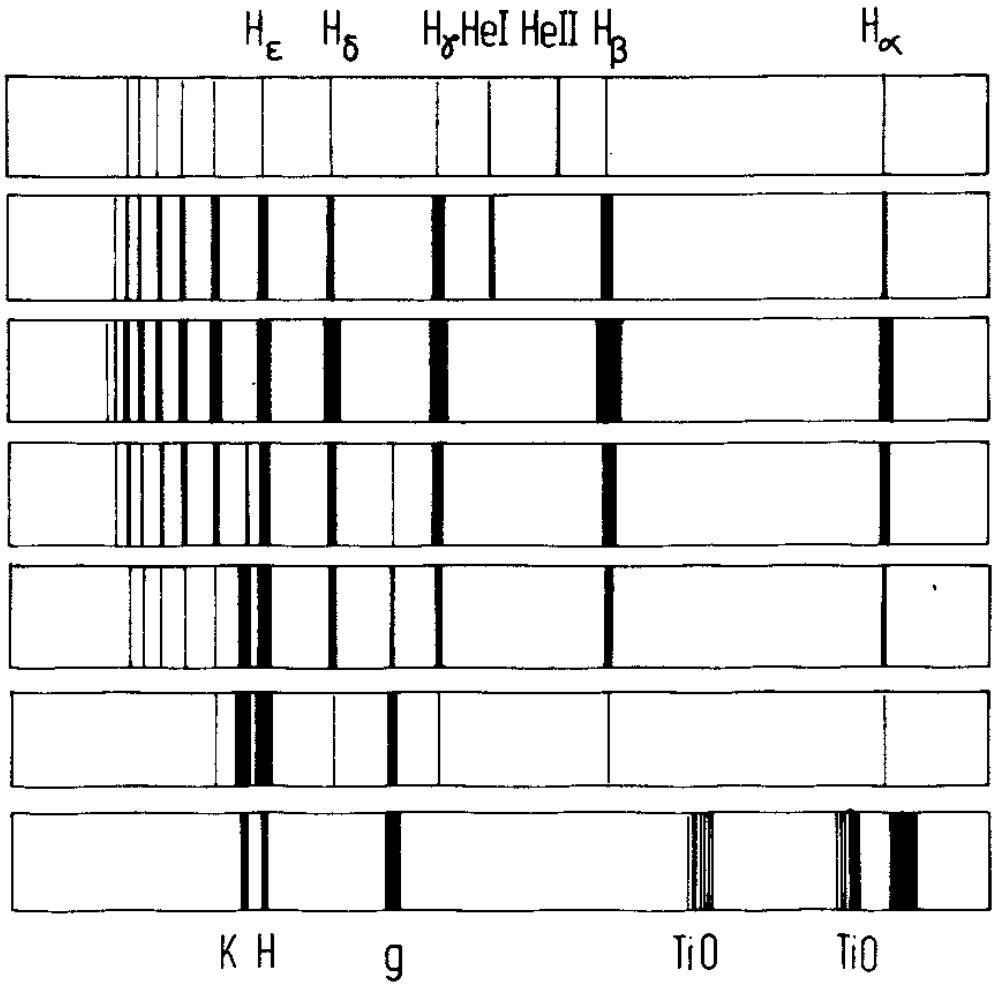

Abb. I.21: Schematische Darstellung der Spektralsequenz.

Scheffler & Elsässer, Physik der Sterne und der Sonne

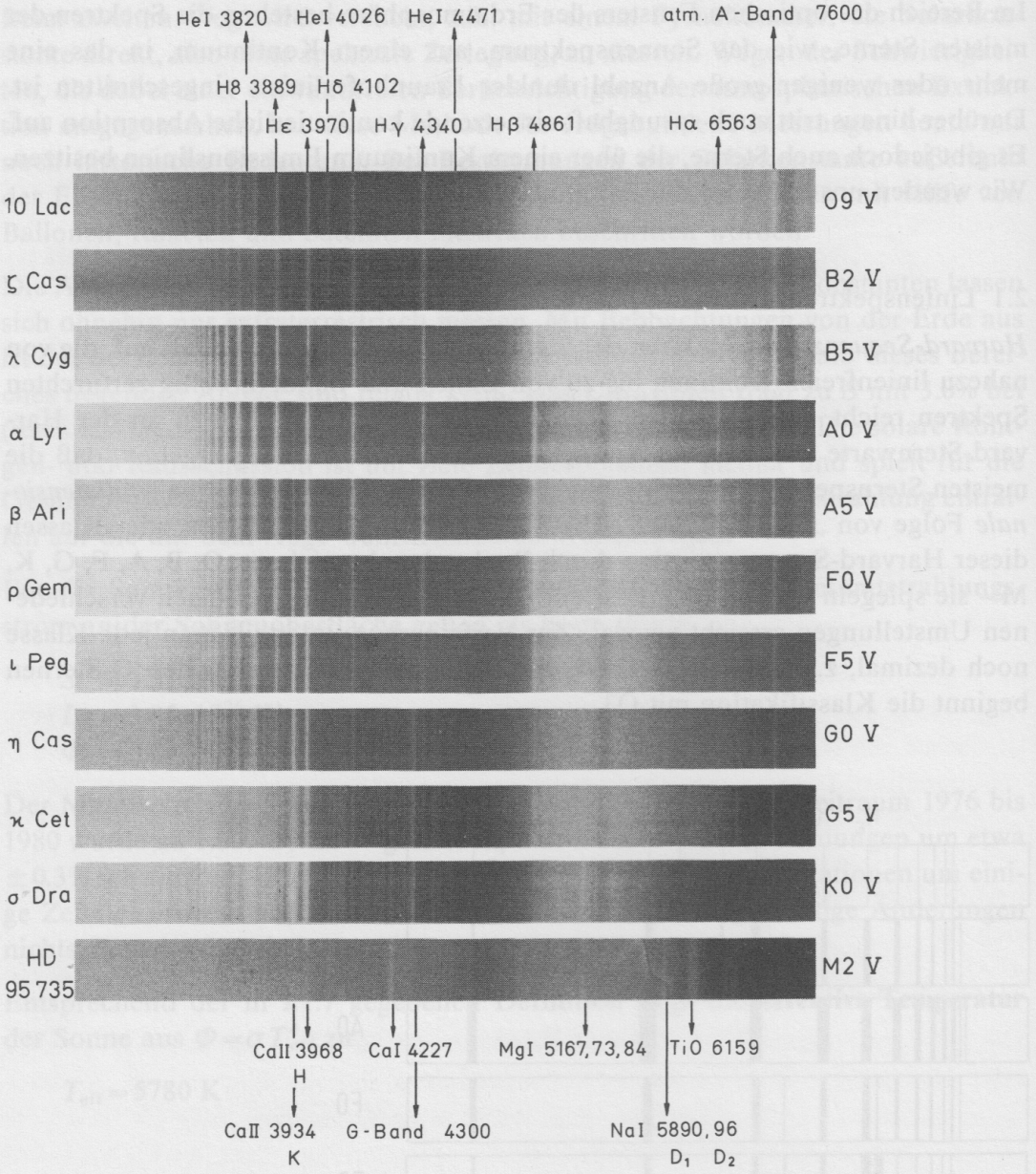

Abb. I.22a: Die Spektralklassen der Hauptreihe (Leuchtkraftklasse V, siehe I.2.10) repräsentiert durch Objektivprismenspektren ausgewählter Sterne (W. Seitter). Die Aufhellungen im Kontinuum zwischen 5000 und 6500 Å ergeben sich durch eine Empfindlichkeitslücke („Grünlücke") des verwendeten Photomaterials.

Scheffler & Elsässer,
Physik der Sterne und der Sonne

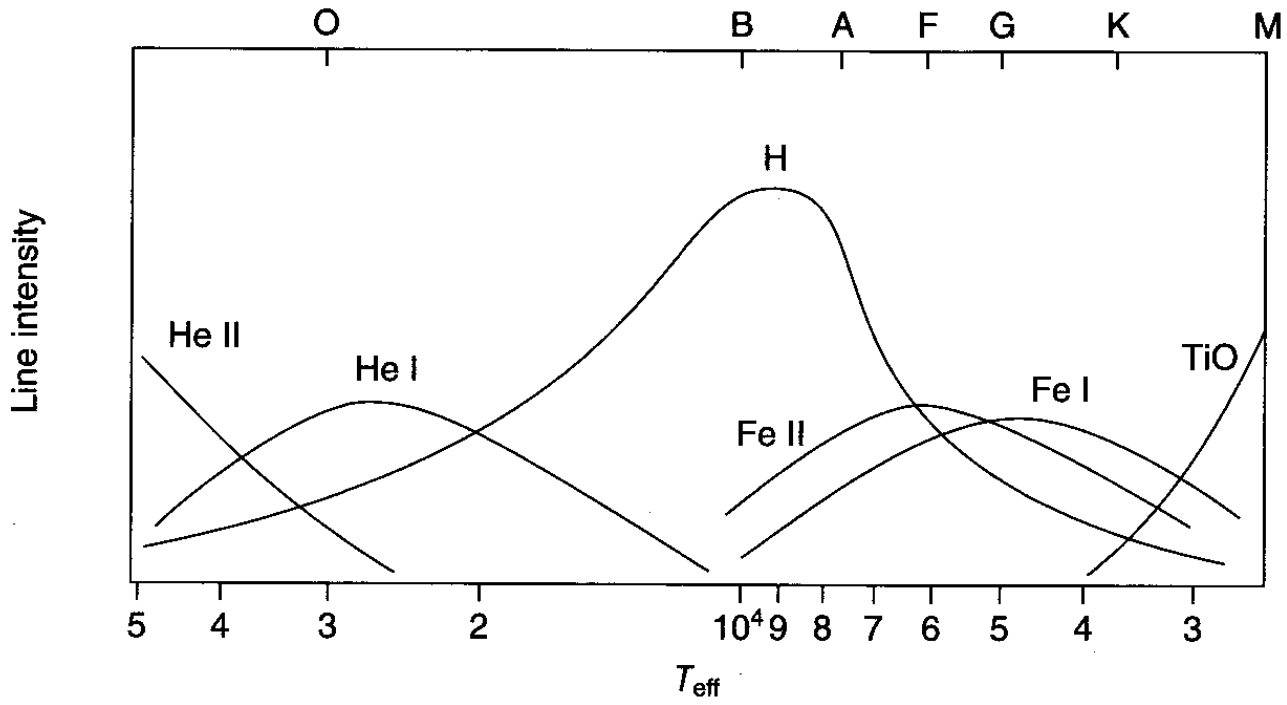

Figure 1.9 Approximate line intensity as a function of T_{eff} for several ions. The spectral types (these are positioned at the coolest temperature for each class) and the intensity of the TiO molecular bands are also shown.

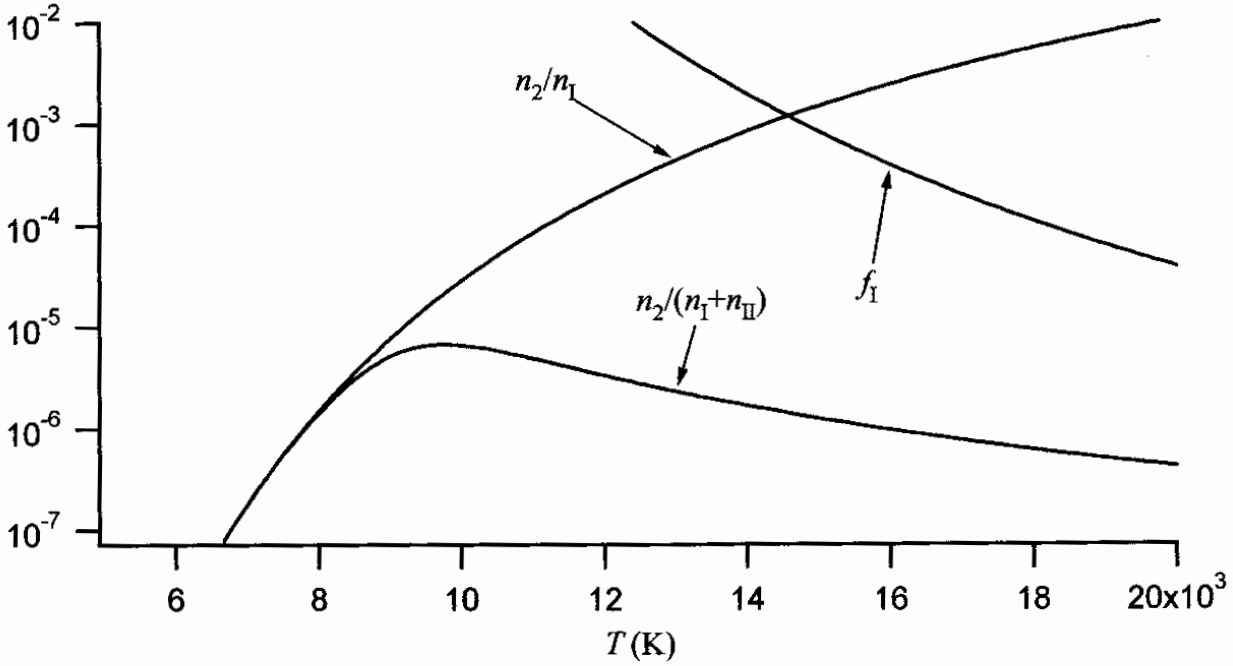

Figure 1.10 Illustration showing the portion of neutral hydrogen atoms found in the $n = 2$ level (n_2/n_I), the neutral ionisation fraction ($f_I = \frac{n_I}{n_I + n_{II}}$) and the product of these two factors that give the portion of all hydrogen atoms found in the $n = 2$ level (i.e. $\frac{n_2}{n_I + n_{II}}$).

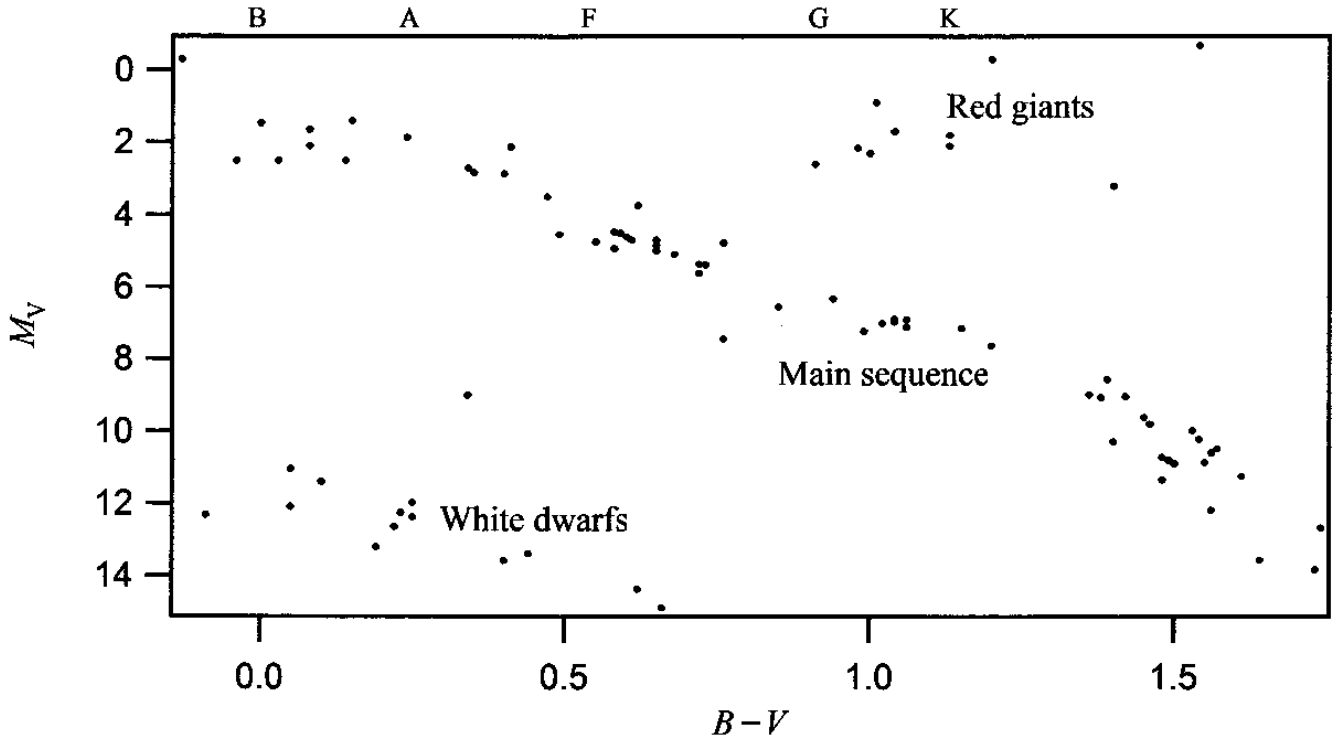

Figure 1.11 A sample taken among the 1000 nearest stars on a color-magnitude H–R diagram. The spectral types are also shown (these are positioned at the coolest temperature for each class).

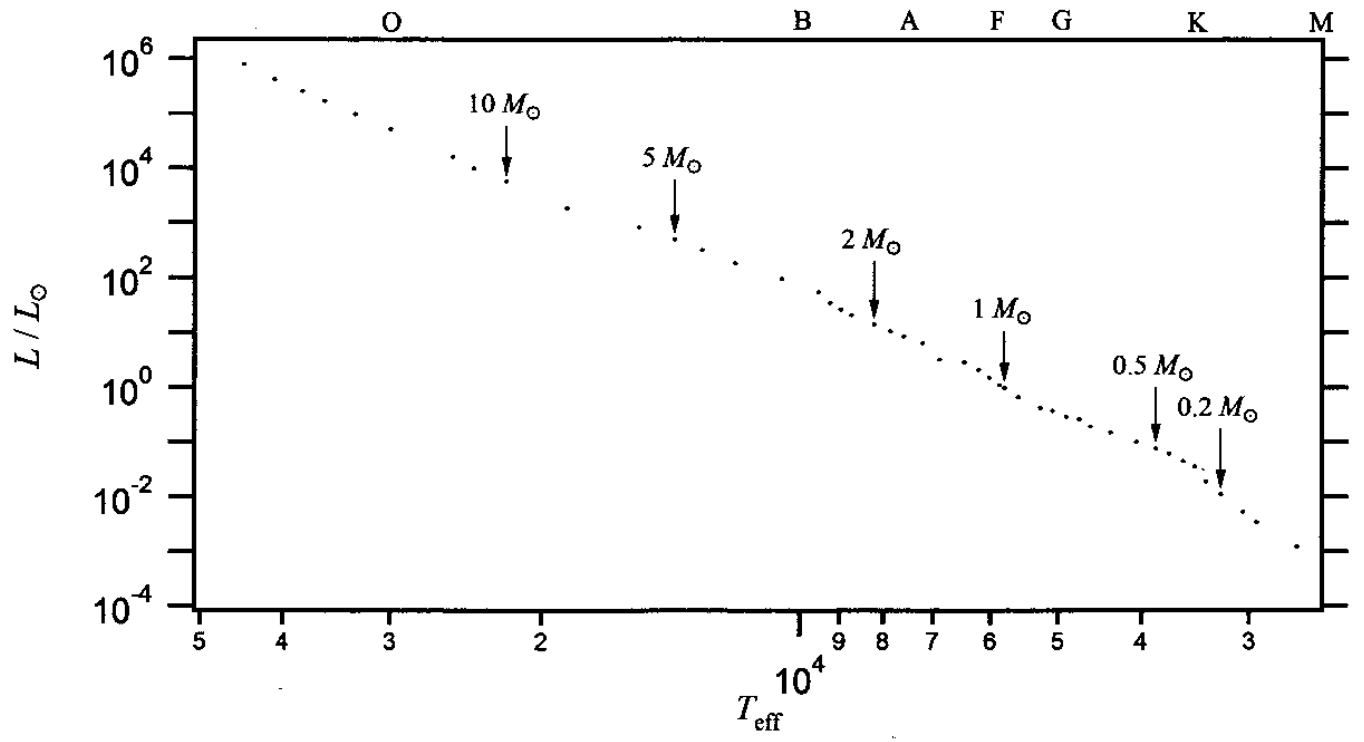

Figure 1.12 The main sequence on an H–R diagram. Several values of the mass are given. The spectral types are also shown (these are positioned at the coolest temperature for each class).

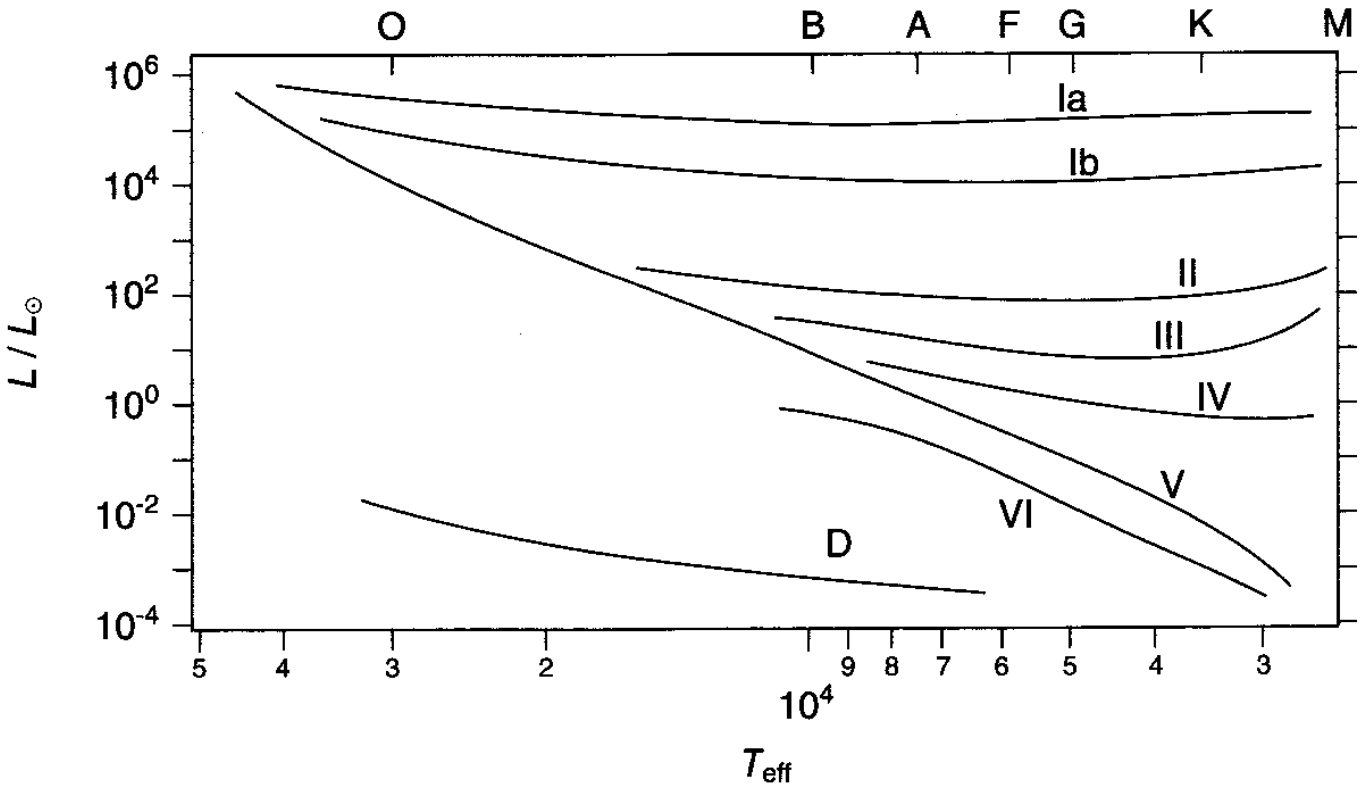

Figure 1.14 Luminosity classes of the H–R diagram. These are identified in Table 1.7. The spectral types are also shown (these are positioned at the coolest temperature for each class).

Table 1.7 Luminosity classes.

Ia	Bright supergiants
Ib	Supergiants
II	Bright giants
III	Giants
IV	Subgiants
V	Main-sequence stars (or dwarfs)
VI (or sd)	Subdwarfs
D (or VII)	White dwarfs

Spectral type	T_{eff} (K)	$M/M_{\odot}$	$L/L_{\odot}$	$R/R_{\odot}$
O5	42 000	60	400 000	12
B0	30 000	17.5	40 000	7.4
B5	15 200	5.9	730	3.9
B8	11 400	3.8	140	3.0
A0	9790	2.9	48	2.4
A5	8180	2.0	12	1.7
F0	7300	1.6	5.7	1.5
F5	6650	1.4	3.0	1.3
G0	5940	1.05	1.4	1.1
G5	5560	0.92	0.73	0.92
K0	5150	0.79	0.46	0.85
K5	4410	0.67	0.18	0.72
M0	3840	0.51	0.070	0.60
M2	3520	0.40	0.034	0.50
M5	3170	0.21	0.0066	0.27

LeBlanc – An Introduction to Stellar Astrophysics